AD-A118 112 ILLINOIS UNIV AT URBANA ELECTROMAGNETICS LAB F/G 9/1
ANALYSIS OF FIN-LINE AT MILLIMETER WAVELENGTHS.(U)
JUL 82 J S WILSON, R MITTRA DAAG29-82-K-0084
UNCLASSIFIED UIEM-82-6 ARO-18054.2-EL NL

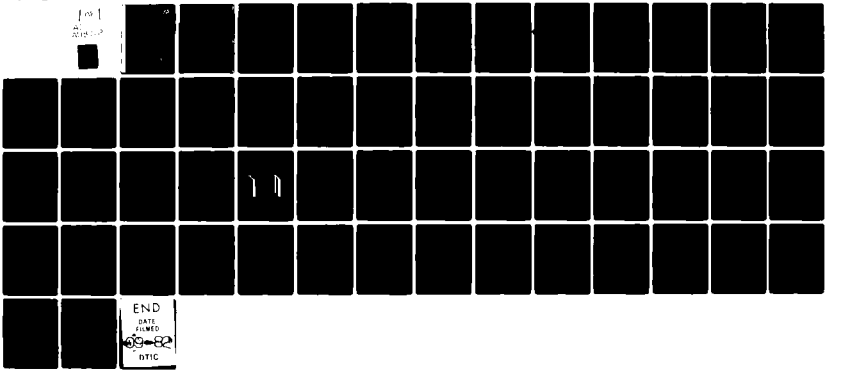

END
DATE FILMED
DTIC

ANALYSIS OF FIN-LINE AT MILLIMETER WAVELENGTHS

INTERIM TECHNICAL REPORT

J. S. Wilson

R. Mittra

July 1982

U. S. ARMY RESEARCH OFFICE

GRANT NO. DAAG29-82-K-0084

ELECTROMAGNETICS LABORATORY
DEPARTMENT OF ELECTRICAL ENGINEERING
ENGINEERING EXPERIMENT STATION
UNIVERSITY OF ILLINOIS AT URBANA-CHAMPAIGN
URBANA, ILLINOIS 61801

APPROVED FOR PUBLIC RELEASE.
DISTRIBUTION UNLIMITED.

THE FINDINGS IN THIS REPORT ARE NOT TO BE CONSTRUED AS AN OFFICIAL DEPARTMENT OF THE ARMY POSITION, UNLESS SO DESIGNATED BY OTHER AUTHORIZED DOCUMENTS.

UNCLASSIFIED

SECURITY CLASSIFICATION OF THIS PAGE (When Data Entered)

REPORT DOCUMENTATION PAGE	READ INSTRUCTIONS BEFORE COMPLETING FORM
1. REPORT NUMBER	2. GOVT ACCESSION NO. AD A118112	3. RECIPIENT'S CATALOG NUMBER
4. TITLE (and Subtitle) ANALYSIS OF FIN-LINE AT MILLIMETER WAVELENGTHS	5. TYPE OF REPORT & PERIOD COVERED Interim Technical Report
	6. PERFORMING ORG. REPORT NUMBER EM 82-6; UILU-ENG-82-2545
7. AUTHOR(s) J. S. Wilson, R. Mittra	8. CONTRACT OR GRANT NUMBER(s) DAAG 29-82-K-0084
9. PERFORMING ORGANIZATION NAME AND ADDRESS Electromagnetics Laboratory, Department of Electrical Engineering, University of Illinois, Urbana, Illinois 61801	10. PROGRAM ELEMENT, PROJECT, TASK AREA & WORK UNIT NUMBERS P18054-EL
11. CONTROLLING OFFICE NAME AND ADDRESS U. S. Army Research Office, Post Office Box 12211, Research Triangle Park, NC 27709	12. REPORT DATE July 1982
	13. NUMBER OF PAGES 54
14. MONITORING AGENCY NAME & ADDRESS (If different from Controlling Office)	15. SECURITY CLASS. (of this report) UNCLASSIFIED
	15a. DECLASSIFICATION/DOWNGRADING SCHEDULE NA

16. DISTRIBUTION STATEMENT (of this Report)

Approved for public release; distribution unlimited.

17. DISTRIBUTION STATEMENT (of the abstract entered in Block 20, if different from Report)

18. SUPPLEMENTARY NOTES

The findings in this report are not to be construed as an official Department of the Army position, unless so designated by other authorized documents.

19. KEY WORDS (Continue on reverse side if necessary and identify by block number)

Millimeter-Waves, Fin-Line, Waveguides, Propagation Constants, Field Calculation.

20. ABSTRACT (Continue on reverse side if necessary and identify by block number)

An analysis of fin-line is presented along with numerical and experimental results. Dispersion characteristics and field distributions are given for a number of single-mode and multi-mode configurations. Agreement between theory and experiment is shown to be quite good.

DD FORM 1 JAN 73 1473 EDITION OF 1 NOV 65 IS OBSOLETE

UNCLASSIFIED

SECURITY CLASSIFICATION OF THIS PAGE (When Data Entered)

UILU-ENG-82-2545

Electromagnetics Laboratory Report No. 82-6

ANALYSIS OF FIN-LINE AT MILLIMETER WAVELENGTHS

by

J. S. Wilson

R. Mittra

Electromagnetics Laboratory
Department of Electrical Engineering
University of Illinois at Urbana-Champaign
Urbana, Illinois 61801

Scientific Report

July 1982

Supported by

Grant No. DAAG 29-82-K-0084
U.S. Army Research Office
P.O. Box 12211
Research Triangle Park, North Carolina 27709

ABSTRACT

An analysis of fin-line is presented along with numerical and experimental results. Dispersion characteristics and field distributions are given for a number of single-mode and multi-mode configurations. Agreement between theory and experiment is shown to be quite good.

TABLE OF CONTENTS

LIST OF FIGURES

I. INTRODUCTION

The need for electronic circuitry operating above 30 GHz has led to the development of a number of waveguide structures. Dielectric waveguide, strip-line, and slot-line have been developed in order to reduce cost, simplify manufacturing processes, reduce loss, and improve adaptability to circuit components. In recent years fin-line has emerged as a viable alternative to these waveguide structures.

Fin-line is the shielded version of slot-line. It consists of a dielectric substrate metalized on one or both sides, a slot is etched in the metal parallel to the direction of propagation, and the structure is surrounded by a metal shield. If the dielectric constant of the substrate equals that of free space, fin-line reduces to ridge-loaded waveguide. If the width of the slot equals the width of the shield, the structure becomes slab-loaded waveguide. There are three types of fin-line: bilateral fin-line, which consists of two sets of metal fins one on each side of the substrate; unilateral fin-line, where the metal fins are on one side of the substrate, and antipodal fin-line, where the upper fin is on one side of the substrate and the lower fin is on the other side of the substrate. The analysis below is restricted to unilateral fin-line; a cross-section view is shown in figure 1.

The structure was first proposed by Meier.[1] Since then several authors have investigated the dispersion characteristics of

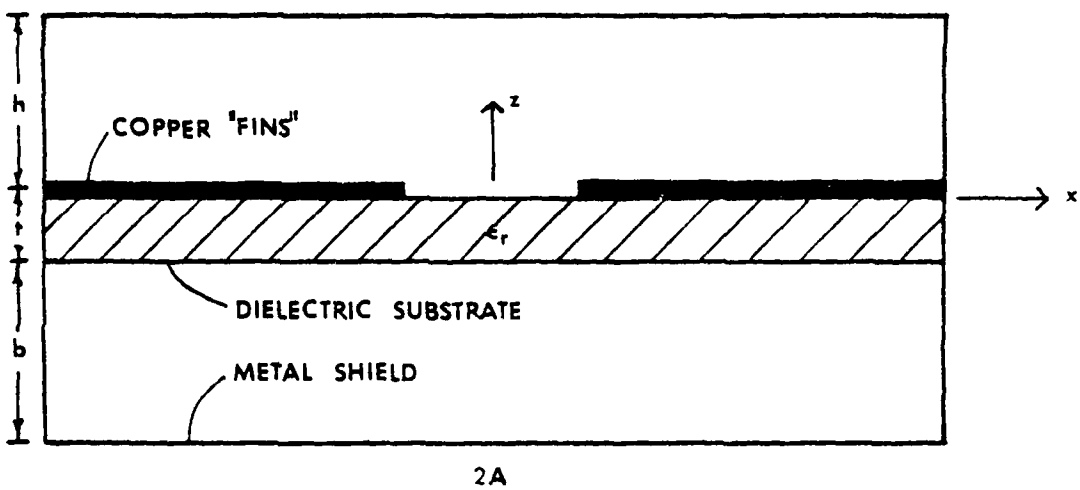

2A

Figure 1. Unilateral Fin-line Geometry

fin-line.[2-9] Recent theoretical approaches involve a spectral domain technique.[6,7] The propagation constant is found using a system of algebraic equations rather than the coupled integral equations used in a space domain solution. The theoretical analysis given below is a spectral domain approach developed by Hayashi, Mittra and Farr.[9]

One of the advantages of fin-line is its adaptability to millimeter wave components. Several authors have reported using fin-line in the fabrication of millimeter wave components including couplers, filters, tapers, detectors, switches, modulators, mixers and oscillators.[2,4,10-13]

In this paper the dispersion characteristics for a variety of configurations are calculated. For two single mode configurations the dispersion characteristics are compared with measured values and agreement is shown to be quite good. Propagation constants are measured for four multi-mode configurations, and field distributions are given for a number of single-mode and multi-mode cases.

A variety of approaches has been used to determine fin-line dispersion characteristics, and agreement between theories is very good, yet experimental verification has only been reported in a few select cases.

Single-mode operation above 100 GHz becomes increasingly difficult due to the small shield sizes required. The use of fin-line at these frequencies need not be restricted if the effects of higher order modes are understood and can be incorporated into the design of fin-line and fin-line components. The results given

below are an initial attempt at characterizing these higher order mode effects.

Field distributions are useful in the design of various fin-line components, yet little has been reported in the literature on field distributions. The results given below may be used in the design of components such as couplers or field displacement devices.

II. THEORETICAL ANALYSIS

A. Derivation of the Determinantal Equation

The fin-line geometry used in the analysis below is shown in figure 1. To arrive at the determinantal equation the fields are given in the spectral domain as an expansion in an infinite set of orthonormal modes. The steady-state Maxwell vector field equations are transformed into modal transmission line equations. The transmission line equations are solved in the three regions (1) $0 \leq z \leq h$, (2) $-t \leq z \leq 0$, and (3) $-(t+b) \leq z \leq -t$. Finally, the boundary conditions required at the various interfaces are applied resulting in the determinantal equation.

Assuming $e^{j\omega t}$ time dependence the field equations are:

$$\nabla \times \vec{E} = -j\omega\mu_o\vec{H} \qquad \nabla \times \vec{H} = j\omega\epsilon\vec{E} \tag{1}$$

where:

$$\epsilon = \begin{cases} \epsilon_o\epsilon_r & -t \leq z \leq 0 \\ \epsilon_o & \text{otherwise} \end{cases}$$

Taking the vector and scalar products of the above equations with the unit vector in the z-direction, the z-components of the fields can be expressed in terms of the transverse components:

$$E_z = \frac{1}{j\omega\epsilon} \nabla \cdot (\vec{H}_t \times \hat{z}) \qquad H_z = \frac{1}{j\omega\mu_o} \nabla \cdot (\hat{z} \times \vec{E}_t) \tag{2}$$

where $\hat{z}$ is the unit vector in the z-direction, and $\vec{E}_t$, $\vec{H}_t$ are the components of the fields transverse to . Since the fields are proportional to $e^{-j\beta y}$, knowing the transverse fields over a plane y = constant allows calculation of all six field components anywhere.

The transverse components of the fields are:

$$\left.\begin{matrix}\vec{E}_t \\ \vec{H}_t\end{matrix}\right\} = \frac{1}{\sqrt{2\pi}} \int_{-\infty}^{\infty} \sum_{m=0}^{\infty} \sum_{\ell=1}^{2} \left\{\begin{matrix} V_{\ell m}(\beta,z)\ \hat{e}_{\ell m}(\beta,x) \\ \\ I_{\ell m}(\beta,z)\ \hat{h}_{\ell m}(\beta,x)\end{matrix}\right\} e^{-j\beta y}\, d\beta \qquad (3)$$

where $\hat{e}_{\ell m}$, $\hat{h}_{\ell m}$ are vector mode functions given by:

$$\hat{e}_{1m} = \frac{\eta_{om}}{2A} \frac{1}{K_m} \left\{-\hat{x}\ \gamma_m \cos \gamma_m(x + A) + \hat{y} j\beta \sin\gamma_m(x + A)\right\} \qquad (4.A)$$

$$\hat{e}_{2m} = \frac{\eta_{om}}{2A} \frac{1}{K_m} \left\{\hat{x}\ j\beta \cos \gamma_m(x + A) - \hat{y}\gamma_m \sin\gamma_m(x + A)\right\} \qquad (4.B)$$

where:

$$\hat{h}_{\ell m} = \hat{z} \times \hat{e}_{\ell m}$$

$$K_m^2 = \gamma_m^2 + \beta^2 \qquad \gamma_m = \frac{m\pi}{2A}$$

$$\eta_{om} = \begin{cases} 1 & m = 0 \\ 2 & m \neq 0 \end{cases}$$

$$\ell = \begin{cases} 1 & \text{E Wave} \quad (H_z \equiv 0) \\ 2 & \text{H Wave} \quad (E_z \equiv 0) \end{cases}$$

The functions $\hat{e}_{\ell m}$, $\hat{h}_{\ell m}$; (1) represent either E wave or H wave with respect to the z-direction, (2) satisfy boundary conditions at $x = \pm A$, (3) are orthonormal.

Substituting equation (3) into equation (2):

$$\left.\begin{matrix} E_z \\ H_z \end{matrix}\right\} = \frac{1}{\sqrt{2\pi}} \int_{-\infty}^{\infty} \sum_{m=0}^{\infty} \left\{ \begin{matrix} \frac{1}{j\omega\epsilon} I_{1m}(\beta,z)\ \nabla_t \cdot [\hat{e}_{1m}(\beta,x)\ e^{-j\beta y}] \\ \\ \frac{1}{j\omega\mu_o} V_{2m}(\beta,z)\ \nabla_t \cdot [\hat{h}_{2m}(\beta,x)\ e^{-j\beta y}] \end{matrix} \right\} d\beta \tag{5}$$

Again taking the scalar and vector products of equation (1) with the unit vector in the z-direction, eliminating the z-components of the fields, and using the properties of the vector mode functions, the resulting expressions are:

$$-\frac{\partial}{\partial z} V_{\ell m}(\beta,z) = jk_m Z_{\ell m} I_{\ell m}(\beta,z) \tag{6.A}$$

$$-\frac{\partial}{\partial z} I_{\ell m}(\beta,z) = jk_m Y_{\ell m} V_{\ell m}(\beta,z) \tag{6.B}$$

where:

$$Z_{1m} = \frac{k_m}{\omega\epsilon} \qquad Z_{2m} = \frac{\omega\mu_o}{k_m}$$

$$Y_{\ell m} = \frac{1}{Z_{\ell m}} \qquad k_m = \sqrt{k^2 - K_m^2}$$

$$k^2 = \begin{cases} \omega^2\mu_o\epsilon_o\epsilon_r & -t \le z \le 0 \\ \\ \omega^2\mu_o\epsilon_o & \text{otherwise} \end{cases}$$

Solving equation (6) in the three regions; (1) $0 \leq z \leq h$, (2) $-t \leq z \leq 0$, and (3) $-(t+b) \leq z \leq 0$, and applying the boundary conditions at $z = h$, $z = -t$, and $z = -(t+b)$ give expressions for $V_{\ell m}$ and $I_{\ell m}$ in the three regions:

i) $z \geq 0$

$$V_{1m} = \upsilon_{1m} \frac{\sin k_{am}(z - h)}{\sin k_{am}h} \tag{7.A}$$

$$I_{1m} = -\upsilon_{1m} \frac{j\omega\epsilon_o}{k_{am}} \frac{\cos k_{am}(z - h)}{\sin k_{am}h} \tag{7.B}$$

$$V_{2m} = -\upsilon_{2m} \frac{\sin k_{am}(z - h)}{\sin k_{am}h} \tag{7.C}$$

$$I_{2m} = -\upsilon_{2m} \frac{jk_{am}}{\omega\mu_o} \frac{\cos k_{am}(z - h)}{\sin k_{am}h} \tag{7.D}$$

ii) $-t \leq z \leq 0$

$$V_{1m} = \upsilon_{1m} \cos k_{dm}z \left\{ \frac{F_{1m}}{\tan k_{dm}t} \tan k_{dm}z + 1 \right\} \tag{7.E}$$

$$I_{1m} = \upsilon_{1m} \frac{j\omega\epsilon_o\epsilon_r}{k_{dm}} \left\{ \frac{F_{1m}}{\tan k_{dm}t} - \tan k_{dm}z \right\} \tag{7.F}$$

$$V_{2m} = \upsilon_{2m} \cos k_{dm}z \left\{ \frac{F_{2m}}{\tan k_{dm}t} \tan k_{dm}z + 1 \right\} \tag{7.G}$$

$$I_{2m} = \upsilon_{2m} \frac{jk_{dm}}{\omega\mu_o} \left\{ \frac{F_{2m}}{\tan k_{dm}t} - \tan k_{dm}z \right\} \tag{7.H}$$

$$F_{1m} = \frac{1 - \frac{\varepsilon_r k_{am}}{k_{dm}} \tanh k_{dm} t \tanh k_{am} b}{1 + \frac{\varepsilon_r k_{am}}{k_{dm}} \frac{\tanh k_{am} b}{\tanh k_{dm} t}} \tag{7.I}$$

$$F_{2m} = \frac{1 - \frac{k_{dm}}{k_{am}} \tanh k_{am} b \tanh k_{dm} t}{1 + \frac{k_{dm}}{k_{am}} \frac{\tanh k_{am} b}{\tanh k_{dm} t}} \tag{7.J}$$

iii) $-(t+b) \leq z \leq -t$

$$V_{1m} = \upsilon_{1m} \frac{G_{1m} \sin k_{am}(z + b + t)}{\sin k_{am} b \cos k_{dm} t} \tag{7.K}$$

$$I_{1m} = \upsilon_{1m} \frac{j\omega\varepsilon_o G_{1m} \cos k_{am}(z + b + t)}{k_{am} \sin k_{am} b \cos k_{dm} t} \tag{7.L}$$

$$V_{2m} = \upsilon_{2m} \frac{G_{2m} \sin k_{am}(z + b + t)}{\sin k_{am} b \cos k_{dm} t} \tag{7.M}$$

$$I_{2m} = \upsilon_{2m} \frac{j}{\omega\mu_o} \frac{G_{2m} \cos k_{am}(z + b + t)}{\sin k_{am} b \cos k_{dm} t} \tag{7.N}$$

$$G_{1m} = \frac{\varepsilon_r k_{am} \tan k_{am} b}{k_{dm} \tan k_{dm} t + \varepsilon_r k_{am} \tan k_{am} b} \tag{7.O}$$

$$G_{2m} = \frac{\frac{1}{k_{am}} \tan k_{am} b}{\frac{1}{k_{am}} \tan k_{am} b + \frac{1}{k_{dm}} \tan k_{dm} t} \tag{7.P}$$

where:

$$k_{am} = \sqrt{k_0^2 - K_m^2} \qquad , \qquad k_{dm} = \sqrt{k^2 - K_m^2}$$

$$\upsilon_{\ell m} = V_{\ell m}(z = 0)$$

$$= \frac{1}{\sqrt{2\pi}} \int_{-A}^{A} dx' \int_{-\infty}^{\infty} dy' \, \hat{h}^{*}_{\ell m}(\beta, x') \cdot \hat{z} \times \vec{\varepsilon}_t(x', y') \, e^{j\beta y'} \qquad (8)$$

$\vec{\varepsilon}_t$ is the unknown transverse component of the electric field at the slot surface.

Substituting equation (7) into equation (3) the transverse magnetic field at the slot surface ($z = 0^+$ and $z = 0^-$) is:

$$\vec{H}_t\Big|_{z=0^+} = \frac{-1}{\sqrt{2\pi}} \int_{-\infty}^{\infty} \sum_{m=0}^{\infty} \left\{ \upsilon_{1m} \frac{j\omega\varepsilon_o}{k_{am}} \frac{\cos k_{am}(z-h)}{\sin k_{am} h} \hat{h}_{1m}(\beta, x) \right.$$

$$\left. + \upsilon_{2m} \frac{jk_{am}}{\omega\mu_o} \frac{\cos k_{am}(z-h)}{\sin k_{am} h} \hat{h}_{2m}(\beta, x) \right\} e^{-j\beta y} \, d\beta \qquad (9.A)$$

$$\vec{H}_t\Big|_{z=0^-} = \frac{1}{\sqrt{2\pi}} \int_{-\infty}^{\infty} \sum_{m=0}^{\infty} \left\{ \upsilon_{1m} \frac{j\omega\varepsilon_o\varepsilon_r}{k_{dm}} \frac{1 - \frac{\varepsilon_r k_{am}}{k_{dm}} \tanh k_{am} b \tanh k_{dm} t}{\tanh k_{dm} t + \frac{\varepsilon_r k_{am}}{k_{dm}} \tanh k_{am} b} \hat{h}_{1m} \right.$$

$$\left. + \upsilon_{2m} \frac{jk_{dm}}{\omega\mu_o} \frac{1 - \frac{k_{dm}}{k_{am}} \tanh k_{am} b \tanh k_{dm} t}{\tanh k_{dm} t + \frac{k_{dm}}{k_{am}} \tanh k_{am} b} \hat{h}_{2m} \right\} e^{-j\beta y} \, d\beta \qquad (9.B)$$

Substituting equation (8) into equation (9) and applying the boundary condition $H_t\Big|_{z=0^+} = H_t\Big|_{z=0^-}$:

$$\sum_{m=0}^{\infty} \iiint \left\{ \left\{ \frac{k_o}{k_{am}} \cot k_{am}h + \frac{\varepsilon_r k_o}{k_{dm}} \frac{1 - \frac{\varepsilon_r k_{am}}{k_{dm}} \tan k_{am}b \tan k_{dm}t}{\tan k_{dm}t + \frac{\varepsilon_r k_{am}}{k_{dm}} \tan k_{am}b} \right\} \cdot \hat{h}_{1m}(\beta,x)\, \hat{h}^*_{1m}(\beta,x') + \left\{ \frac{k_{am}}{k_o} \cot k_{am}h + \frac{k_{dm}}{k_o} \frac{1 - \frac{k_{dm}}{k_{am}} \tanh k_{am}b \tanh k_{dm}t}{\tan k_{dm}t + \frac{k_{dm}}{k_{am}} \tan k_{am}b} \right\} \cdot \hat{h}_{2m}(\beta,x)\, \hat{h}^*_{2m}(\beta,x') \right\} \cdot \vec{M}(x',y')\, e^{-j\beta(y-y')}\, d\beta\, dx'dy' = 0 \qquad (10)$$

where $\vec{M}(x',y') = \hat{z} \times \vec{\varepsilon}_t(x',y')$ is the unknown current density on the slot surface.

Let β_o be the propagation constant of the wave and set:

$$\vec{M}(x',y') = \vec{f}(x')\, e^{-j\beta_o y'}$$

$$= [\hat{x}\, f_x(x') + \hat{y}\, f_y(x')]\, e^{-j\beta_o y'} \qquad (11)$$

Substituting equation (11) into equation (10) and performing the integration over $d\beta$ and dy', equation (10) can be rewritten:

$$\sum_{m=0}^{\infty} \int_{-W}^{W} \left\{ P_{1m}(\beta_o)\, \hat{h}_{1m}(\beta_o,x)\, \hat{h}^*_{1m}(\beta_o,x') + P_{2m}(\beta_o)\, \hat{h}_{2m}(\beta_o,x)\, h^*_{2m}(\beta_o,x') \right\} \cdot \vec{f}(\vec{x}')\, dx' = 0 \qquad (12)$$

where:

$$P_{1m}(\beta) = \frac{k_o}{k_{am}} \cot k_{am}h + \frac{\varepsilon_r k_o}{k_{dm}} \frac{1 - \frac{\varepsilon_r k_{am}}{k_{dm}} \tan k_{am}b \tan k_{dm}t}{\tan k_{dm}t + \frac{\varepsilon_r k_{am}}{k_{dm}} \tan k_{am}b} \qquad (13.A)$$

$$P_{2m}(\beta) = \frac{k_{am}}{k_o} \cot k_{am} h + \frac{k_{dm}}{k_o} \frac{1 - \frac{k_{dm}}{k_{am}} \tan k_{am} b \tan k_{dm} t}{\tan k_{dm} t + \frac{k_{dm}}{k_{am}} \tan k_{am} b} \qquad (13.B)$$

Equation (12) is the determinantal equation.

B. Solution of the Determinantal Equation Using Galerkin's Method

The unknown magnetic current density, equation (11), is expanded in terms of the basis functions $f_{xn}(x')$ and $f_{yn}(x')$:

$$f_x(x') = \sum_{n'=1}^{2N_x} a_{xn'} f_{xn'}(x') \qquad (14.A)$$

$$f_y(x') = \sum_{n'=1}^{2N_y} j\, a_{yn'} f_{yn'}(x') \qquad (14.B)$$

Substituting equation (14) into equation (12), taking the inner product of the x-component with $f_{xn}(x)$, and the inner product of the y-component with $f_{yn}(x)$, equation (12) can be rewritten:

i) x-component

$$\sum_{n'=1}^{2N_x} a_{xn'} \left[\sum_{m=1}^{\infty} \frac{1}{AK_m^2} \left\{ \beta_o^2 P_{1m}(\beta_o) + \gamma_m^2 P_{2m}(\beta_o) \right\} \tilde{f}_{xn} \tilde{f}_{xn'} \right]$$

$$+ \sum_{n'=1}^{2N_y} a_{yn'} \left[\sum_{m=1}^{\infty} \frac{1}{AK_m^2} \beta_o \gamma_m \left\{ P_{2m}(\beta_o) - P_{1m}(\beta_o) \right\} \tilde{f}_{xn} \tilde{f}_{yn'} \right]$$

$$= 0 \qquad n = 1, \ldots, N_x \qquad (15.A)$$

ii) y-component

$$\sum_{n'=1}^{2N_x} a_{xn'} \left[\sum_{m=1}^{\infty} \frac{1}{AK_m^2} \beta_o \gamma_m \left\{ P_{2m}(\beta_o) - P_{1m}(\beta_o) \right\} \tilde{f}_{yn} \tilde{f}_{xn'} \right]$$

$$+ \sum_{n'=1}^{2N_y} a_{yn'} \left[\sum_{m=0}^{\infty} \frac{\eta_{om}}{2AK_m^2} \left\{ \gamma_m^2 P_{1m}(\beta_o) + \beta_o^2 P_{2m}(\beta_o) \right\} \tilde{f}_{yn} \tilde{f}_{yn'} \right]$$

$$= 0 \qquad n = 1, \ldots, N_y \tag{15.B}$$

β_o is a particular value of β, and:

$$\tilde{f}_{xn} = \int_{-W}^{W} \sin \gamma_m(x' + A) \, f_{xn}(x') \, dx' \tag{16.A}$$

$$\tilde{f}_{yn} = \int_{-W}^{W} \cos \gamma_m(x' + A) \, f_{yn}(x') \, dx' \tag{16.B}$$

Equations (15.A) and (15.B) are the simultaneous equations for the unknowns a_{xn} and a_{yn}. In order for equations (15.A) and (15.B) to yield nontrivial solutions the determinant of the coefficients must be zero.

In choosing the basis functions $f_{xn}(x)$ and $f_{yn}(x)$ the following considerations must be taken into account; (1) the y-component of the slot field goes to zero, and the x-component becomes infinite at the edges of the slot, (2) integration of equation (16) is performed analytically, and (3) the solution should converge as the number of basis functions increases. Based upon these considerations, the basis functions are chosen as:

$$f_{xn} = U_n\left(\frac{x}{W}\right) \tag{17.A}$$

$$f_{yn} = \frac{T_{n-1}\left(\frac{x}{W}\right)}{\sqrt{1 - \left(\frac{x}{W}\right)^2}} \tag{17.B}$$

where:

$T_n(z)$ = Chebyshev polynomial of the first kind

$U_n(z)$ = Chebyshev polynomial of the second kind.

Substituting equation (17) into equation (16):

$$\tilde{f}_{xn} = \int_{-W}^{W} \sin \gamma_m(x + A)\, U_n\left(\frac{x}{W}\right)\, dx$$

$$= \begin{cases} (-1)^{n/2-1} \dfrac{n\pi}{\gamma_m} \cos(\gamma_m A)\, J_n(\gamma_m W) & (n = \text{even}) \\ (-1)^{\frac{n-1}{2}} \dfrac{n\pi}{\gamma_m} \sin(\gamma_m A)\, J_n(\gamma_m W) & (n = \text{odd}) \end{cases} \tag{18.A}$$

$$\tilde{f}_{yn} = \int_{-W}^{W} \cos \gamma_m(x + A)\, \frac{T_{n-1}\left(\frac{x}{W}\right)}{\sqrt{1 - \left(\frac{x}{W}\right)^2}}\, dx$$

$$= \begin{cases} (-1)^{\frac{n-1}{2}} W\pi \cos(\gamma_m A)\, J_{n-1}(\gamma_m W) & (n = \text{odd}) \\ (-1)^{n/2} W\pi \sin(\gamma_m A)\, J_{n-1}(\gamma_m W) & (n = \text{even}) \end{cases} \tag{18.B}$$

Substituting equation (18) into equation (15), it is apparent there exist two sets of solutions, one where the odd m terms are nonzero (odd mode), and a second where the even m terms are nonzero (even mode). Rewriting equation (15):

$$\sum_{j=1}^{N_x} F_{ij}^{(11)} a_{xj} + \sum_{j=1}^{N_y} F_{ij}^{(12)} a_{yj} = 0 \qquad (i = 1,\ldots,N_x) \tag{19.A}$$

$$\sum_{j=1}^{N_x} F_{ij}^{(21)} a_{xj} + \sum_{j=1}^{N_y} F_{ij}^{(22)} a_{yj} = 0 \qquad (i = 1,\ldots,N_y) \tag{19.B}$$

The matrix elements are:

i) even mode

$$F_{ij}^{(11)} = (-1)^{i+j}\, 4ij \sum_{m=1}^{\infty} \frac{1}{(K_m \gamma_m W)^2} \left\{ \beta_o^2 P_{1m}(\beta_o) + \gamma_m^2 P_{2m}(\beta_o) \right\} \cdot J_{2i}(\gamma_m W)\, J_{2j}(\gamma_m W) \tag{20.A}$$

$$F_{ij}^{(12)} = (-1)^{i+j}\, 2i \sum_{m=1}^{\infty} \frac{\beta_o \gamma_m}{K_m^2(\gamma_m W)} \left\{ P_{2m}(\beta_o) - P_{1m}(\beta_o) \right\} \cdot J_{2i}(\gamma_m W)\, J_{2j-2}(\gamma_m W) \tag{20.B}$$

$$F_{ij}^{(21)} = F_{ij}^{(12)} \tag{20.C}$$

$$F_{ij}^{(22)} = (-1)^{i+j} \sum_{m=0}^{\infty} \frac{r_{om}}{2K_m^2} \left\{ \gamma_m^2 P_{1m}(\beta_o) + \beta_o^2 P_{2m}(\beta_o) \right\}$$

$$\cdot J_{2i-2}(\gamma_m W)\ J_{2j-2}(\gamma_m W) \tag{20.D}$$

where $\gamma_m = \frac{m\pi}{A}$

ii) odd mode

$$F_{ij}^{(11)} = (-1)^{i+j}(2i-1)(2j-1) \sum_{m=1}^{\infty} \frac{1}{(K_m \gamma_m W)^2} \left\{ \beta_o^2 P_{1m}(\beta_o) + \gamma_m^2 P_{2m}(\beta_o) \right\}$$

$$\cdot J_{2i-1}(\gamma_m W)\ J_{2j-1}(\gamma_m W) \tag{20.E}$$

$$F_{ij}^{(12)} = (-1)^{i+j}\ (2i-1) \sum_{m=1}^{\infty} \frac{\beta_o \gamma_m}{K_m^2 \gamma_m W} \left\{ P_{2m}(\beta_o) - P_{1m}(\beta_o) \right\}$$

$$\cdot J_{2i-1}(\gamma_m W)\ J_{2j-1}(\gamma_m W) \tag{20.F}$$

$$F_{ij}^{(21)} = F_{ij}^{(12)} \tag{20.G}$$

$$F_{ij}^{(22)} = (-1)^{i+j} \sum_{m=1}^{\infty} \frac{1}{K_m^2} \left\{ \gamma_m^2 P_{1m}(\beta_o) + \beta_o^2 P_{2m}(\beta_o) \right\}$$

$$\cdot J_{2i-1}(\gamma_m W)\ J_{2j-1}(\gamma_m W) \tag{20.H}$$

where $\gamma_m = \frac{(2m-1)\pi}{2A}$

A computer program has been written[9] that finds the allowed values β_o by finding the values of β where the determinant of the coefficient matrix is zero.

C. The Field Expressions

Substituting equation (14) into equation (11), equation (11) into equation (8), equation (8) into equation (7), equation (7) into equation (3) and equation (5), and performing the integration over β and y', the six field components are:

$$E_x = j \sum_{m=0}^{\infty} \frac{\eta_{om}}{2A} \frac{1}{K_m^2} \cos\gamma_m(x + A) \left\{ \gamma_m \beta \left\{ T_{2m}^{\upsilon} - T_{1m}^{\upsilon} \right\} \sum_{n=1}^{N_x} a_{xn} \tilde{f}_{xn} + \left\{ \gamma_m^2 T_{1m}^{\upsilon} + \beta^2 T_{2m}^{\upsilon} \right\} \sum_{n=1}^{N_y} a_{yn} \tilde{f}_{yn} \right\} e^{-j\beta y} \Big|_{\beta=\beta_o} \quad (21.A)$$

$$E_y = \sum_{m=0}^{\infty} \frac{\eta_{om}}{2A} \frac{1}{K_m^2} \sin\gamma_m(x + A) \left\{ -\left\{ \beta^2 T_{1m}^{\upsilon} + \gamma_m^2 T_{2m}^{\upsilon} \right\} \sum_{n=1}^{N_x} a_{xn} \tilde{f}_{xn} + \gamma_m \beta \left\{ T_{1m}^{\upsilon} - T_{2m}^{\upsilon} \right\} \sum_{n=1}^{N_y} a_{yn} \tilde{f}_{yn} \right\} e^{-j\beta y} \Big|_{\beta=\beta_o} \quad (21.B)$$

$$E_z = \sum_{m=0}^{\infty} \frac{\eta_{om}}{2A} \frac{1}{j\omega\epsilon} \sin\gamma_m(x + A) \left| Y_{1m} \right| \left\{ \beta \sum_{n=1}^{N_x} a_{xn} \tilde{f}_{xn} - \gamma_m \sum_{n=1}^{N_y} a_{yn} \tilde{f}_{yn} \right\} e^{-j\beta y} \Big|_{\beta=\beta_o} \quad (21.C)$$

$$H_x = j \sum_{m=0}^{\infty} \frac{\eta_{om}}{2A} \frac{1}{K_m^2} \sin\gamma_m(x + A) \left\{ -\left\{ \beta^2 \left| Y_{1m} \right| + \gamma_m^2 \left| Y_{2m} \right| \right\} \right.$$

$$\cdot \sum_{n=1}^{N_x} a_{xn} \tilde{f}_{xn} + \gamma_m \beta \left\{ \left| Y_{1m} \right| - \left| Y_{2m} \right| \right\}$$

$$\left. \cdot \sum_{n=1}^{N_y} a_{yn} \tilde{f}_{yn} \right\} e^{-j\beta y} \Big|_{\beta=\beta_o} \qquad (21.D)$$

$$H_y = \sum_{m=0}^{\infty} \frac{\eta_{om}}{2A} \frac{1}{K_m^2} \cos\gamma_m(x + A) \left\{ \gamma_m \beta \left\{ \left| Y_{2m} \right| - \left| Y_{1m} \right| \right\} \right.$$

$$\cdot \sum_{n=1}^{N_x} a_{xn} \tilde{f}_{xn} + \left\{ \gamma_m^2 \left| Y_{1m} \right| + \beta^2 \left| Y_{2m} \right| \right\}$$

$$\left. \cdot \sum_{n=1}^{N_y} a_{yn} \tilde{f}_{yn} \right\} e^{-j\beta y} \Big|_{\beta=\beta_o} \qquad (21.E)$$

$$H_z = \sum_{m=0}^{\infty} \frac{\eta_{om}}{2A} \frac{1}{j\omega\mu_o} \cos\gamma_m(x + A) \, T_{2m}^{\upsilon} \left\{ \gamma_m \sum_{n=1}^{N_x} a_{xn} \tilde{f}_{xn} \right.$$

$$\left. + \beta \sum_{n=1}^{N_y} a_{yn} \tilde{f}_{yn} \right\} e^{-j\beta y} \Big|_{\beta=\beta_o} \qquad (21.F)$$

where:

$$T_{\ell m}^{\upsilon} = V_{\ell m} / \upsilon_{\ell m}$$

$$\left| Y_{\ell m} \right| = j \, I_{\ell m} / \upsilon_{\ell m}$$

$V_{\ell m}$, $I_{\ell m}$ are given by equation (7).

(1) Even Mode Solutions

From equation (18) the basis functions for the even modes can be written:

$$f_{xn} = \frac{1}{\pi W} U_{2n}\left(\frac{x}{W}\right) \tag{22.A}$$

$$f_{yn} = \frac{1}{\pi W} \frac{T_{2n-2}\left(\frac{x}{W}\right)}{\sqrt{1 - \left(\frac{x}{W}\right)^2}} \tag{22.B}$$

Substituting equation (22) into equation (16):

$$\tilde{f}_{xn} = (-1)^{m+n-1} \frac{2n}{W\gamma_m} J_{2n}(\gamma_m W) \tag{23.A}$$

$$\tilde{f}_{yn} = (-1)^{m+n-1} J_{2n-2}(\gamma_m W) \tag{23.B}$$

Substitution of equation (23) into equation (21) gives the expression used to calculate the field distribution for even mode solutions.

(2) Odd Mode Solutions

From equation (18) the basis functions for the odd modes can be written:

$$f_{xn} = \frac{1}{\pi W} U_{2n-1}\left(\frac{x}{W}\right) \tag{24.A}$$

$$f_{yn} = \frac{1}{\pi W} \frac{T_{2n-1}\left(\frac{x}{W}\right)}{\sqrt{1 - \left(\frac{x}{W}\right)^2}} \tag{24.B}$$

Substituting equation (24) into equation (16):

$$\tilde{f}_{xn} = (-1)^{m+n-1} \frac{(2n-1)}{W\gamma_m} J_{2n-1}(\gamma_m W) \tag{25.A}$$

$$\tilde{f}_{yn} = (-1)^{m+n} J_{2n-1}(\gamma_m W) \tag{25.B}$$

Substitution of equation (25) into equation (21) gives the expression used to calculate the field distribution for odd mode solutions.

III. EXPERIMENTAL RESULTS AND NUMERICAL RESULTS

A. Experiment Procedure

An experiment was performed to measure the propagation constant for various fin-line configurations. The purpose of these measurements was to compare measured and calculated dispersion characteristics for both single-moded and multi-moded cases.

A block diagram of the experiment is shown in figure 2. Details of the sliding short assembly are shown in figure 3. The fin-line is made from 1 oz. copper clad RT/Duroid 5880 with an ε_r of 2.22, and a loss tangent of less than 0.01. The copper is photochemically etched off the duroid; the gap width 2W is kept uniform by using precision width tape. Both ends of the fin-line section are tapered to attain a degree of matching to the metal waveguide.

The short consists of a copper block that fills the upper half of the metal shield; any power transmitted through the lower half of the metal shield is absorbed to prevent multiple reflections. The XY recorder plots the standing wave pattern produced along the fin-line and translated to the detector. The distances between successive minima are measured, and averaged, giving the propagation constant for that plot. A number of plots are made in order to reduce random errors. The result is a value of the propagation constant for a given configuration, at a given frequency. A typical standing wave pattern is illustrated in figure 4.

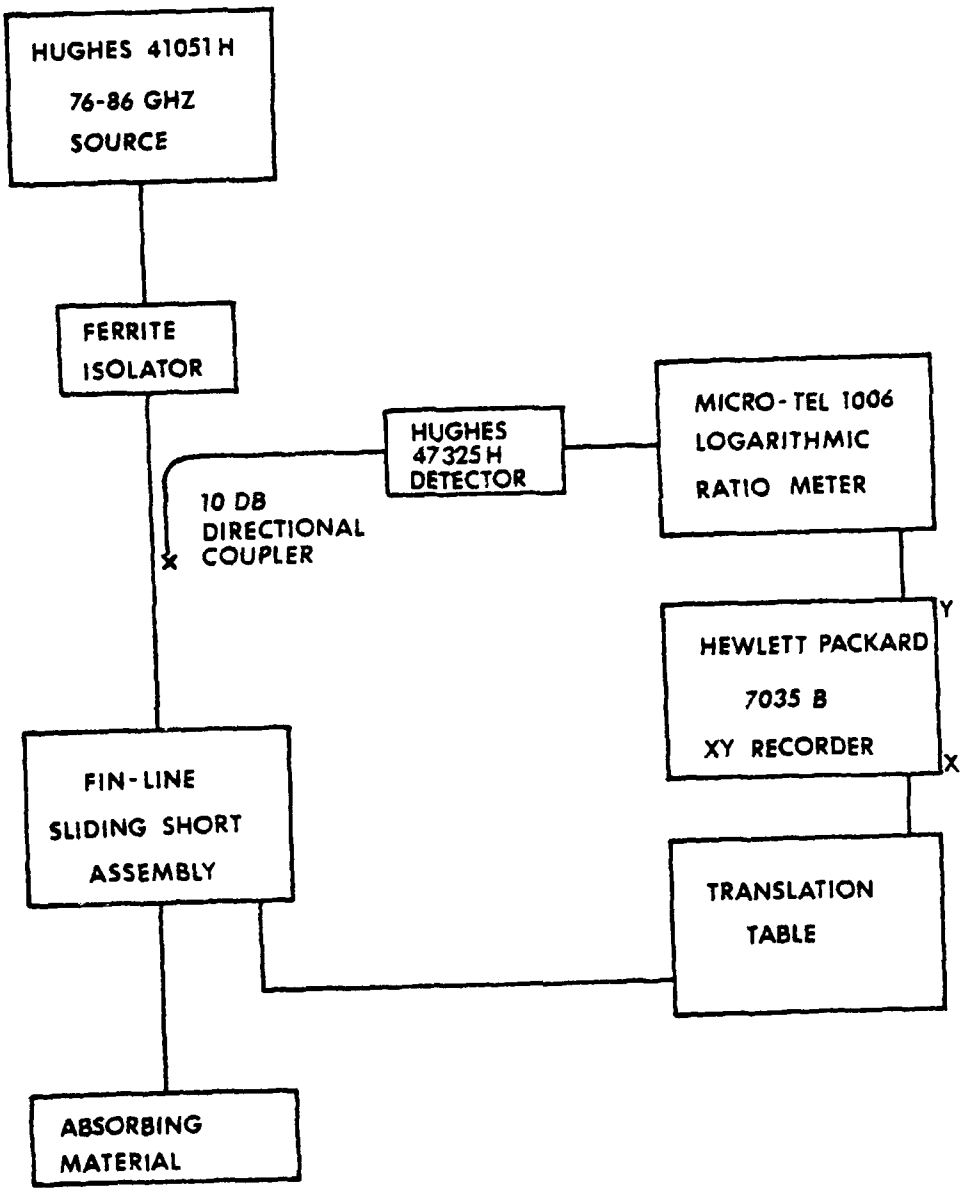

Figure 2. Block Diagram of Experimental Apparatus

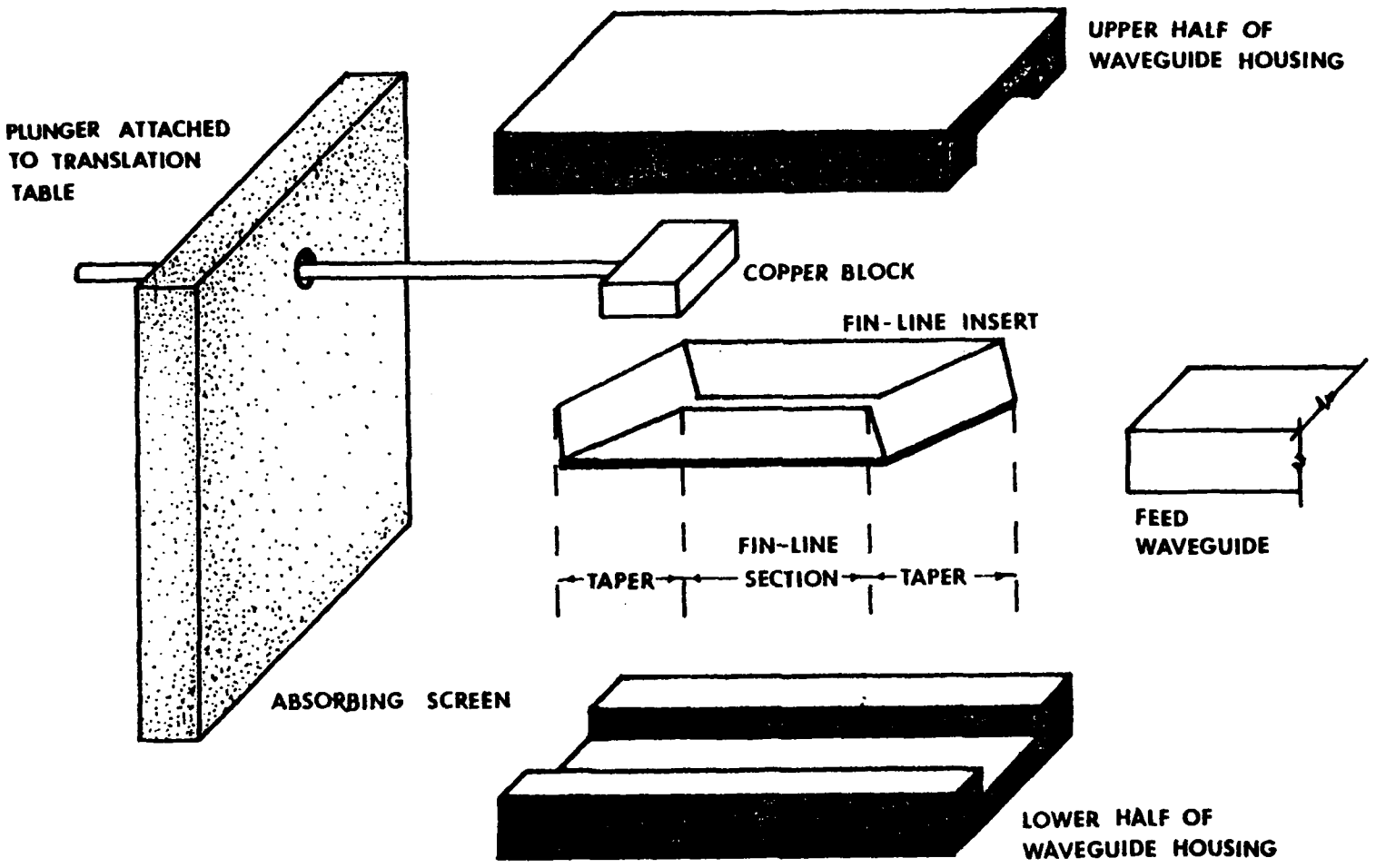

Figure 3. Details of the Sliding-Short Assembly

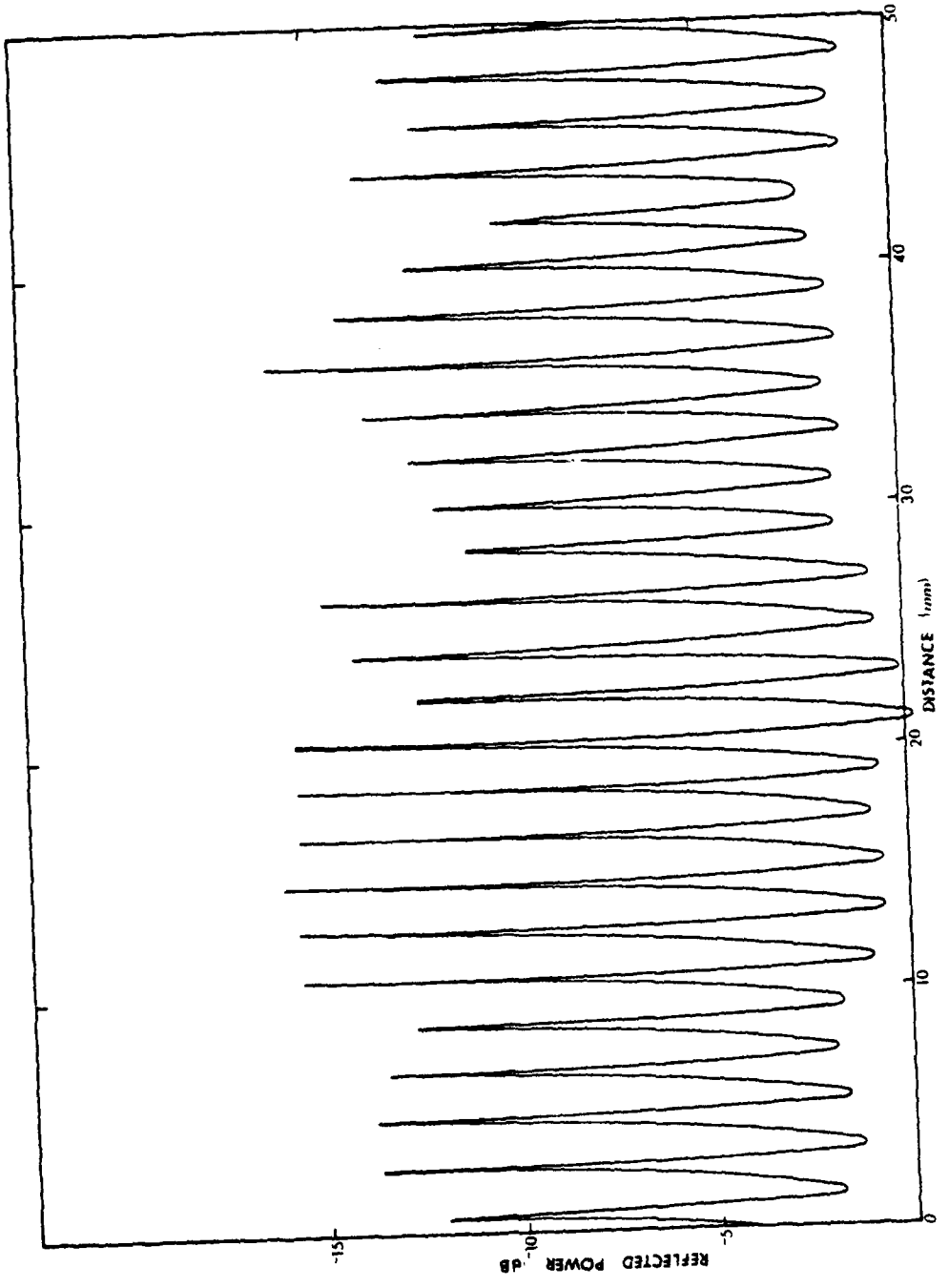

Figure 4. Typical Standing Wave Pattern

B. Experimental Data and Numerical Data Single-Mode Case

Before comparing numerical and experimental data, the accuracy of the computer program was checked by comparing the present theory with previously published results.[7] In figure 5 the normalized propagation constant squared for a typical fin-line configuration is plotted over the single-mode frequency range. There is approximately a two percent discrepancy between the two theories, possibly caused by using different basis functions. Knorr and Shayda use constant amplitudes rather than the Chebyshev polynomials given in equation (22). It is believed the present theory is more accurate because the basis functions more closely resemble the actual gap fields.

Figure 5 also compares dispersion characteristics of a typical fin-line configuration with the equivalent metal waveguide characteristics. The addition of the fin-line increases the single-mode frequency range by approximately ten percent.

Propagation constants were measured over the frequency range 76 to 82 GHz for fin-line shielded in WR12 waveguide. In figure 6 the normalized propagation constant squared is plotted as a function of frequency for two configurations. In figure 7 measured values of the normalized propagation constant squared are shown along with the theoretical curves. For the case $2W = 0.020"$ the experimental values are on an average six percent lower than the calculated values. For the case $2W = 0.050"$ the experimental values are on an average three percent lower than the calculated values.

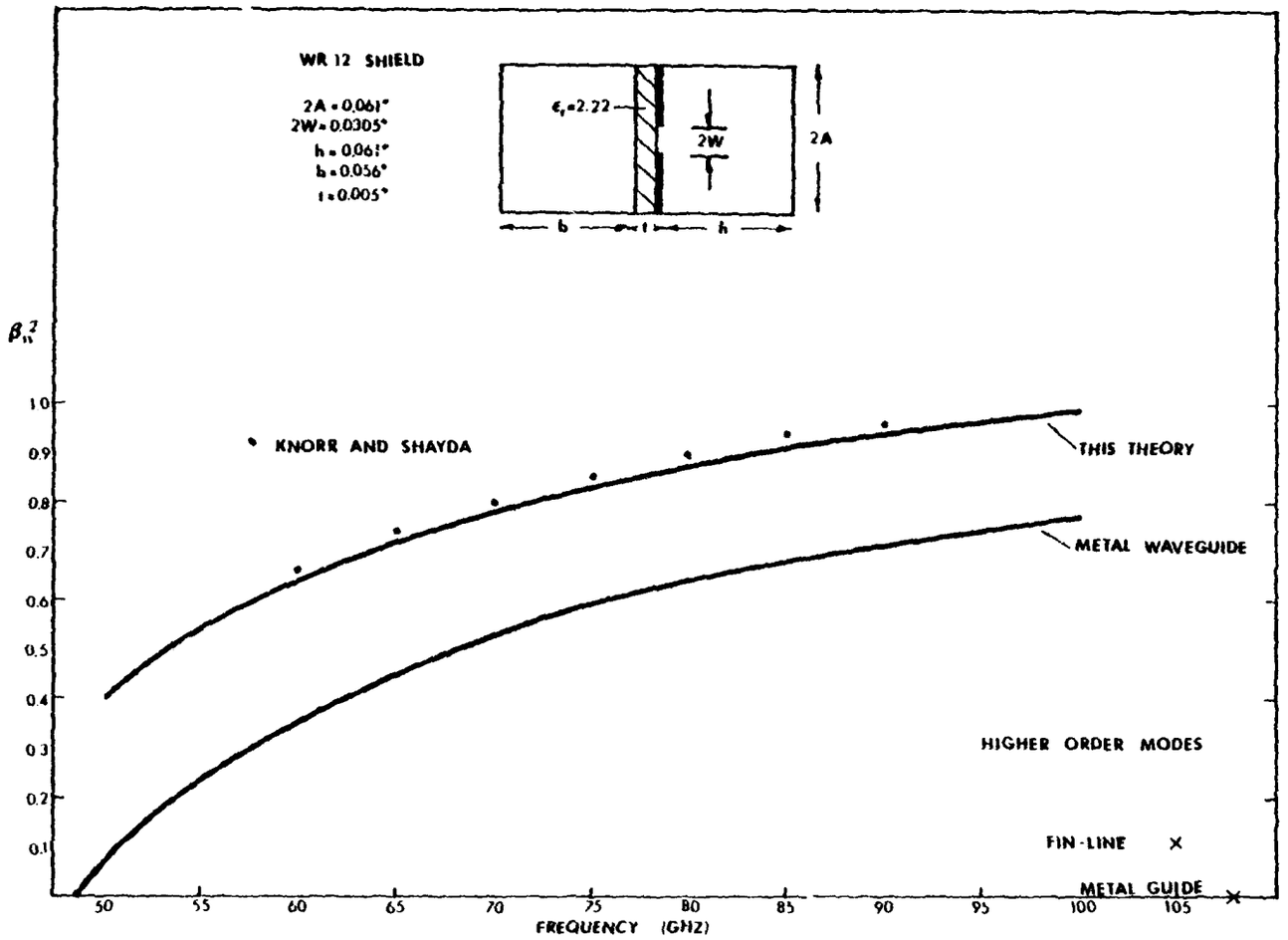

Figure 5. Comparison of Fin-line Dispersion Characteristics with Another Theory and Metal Waveguide.

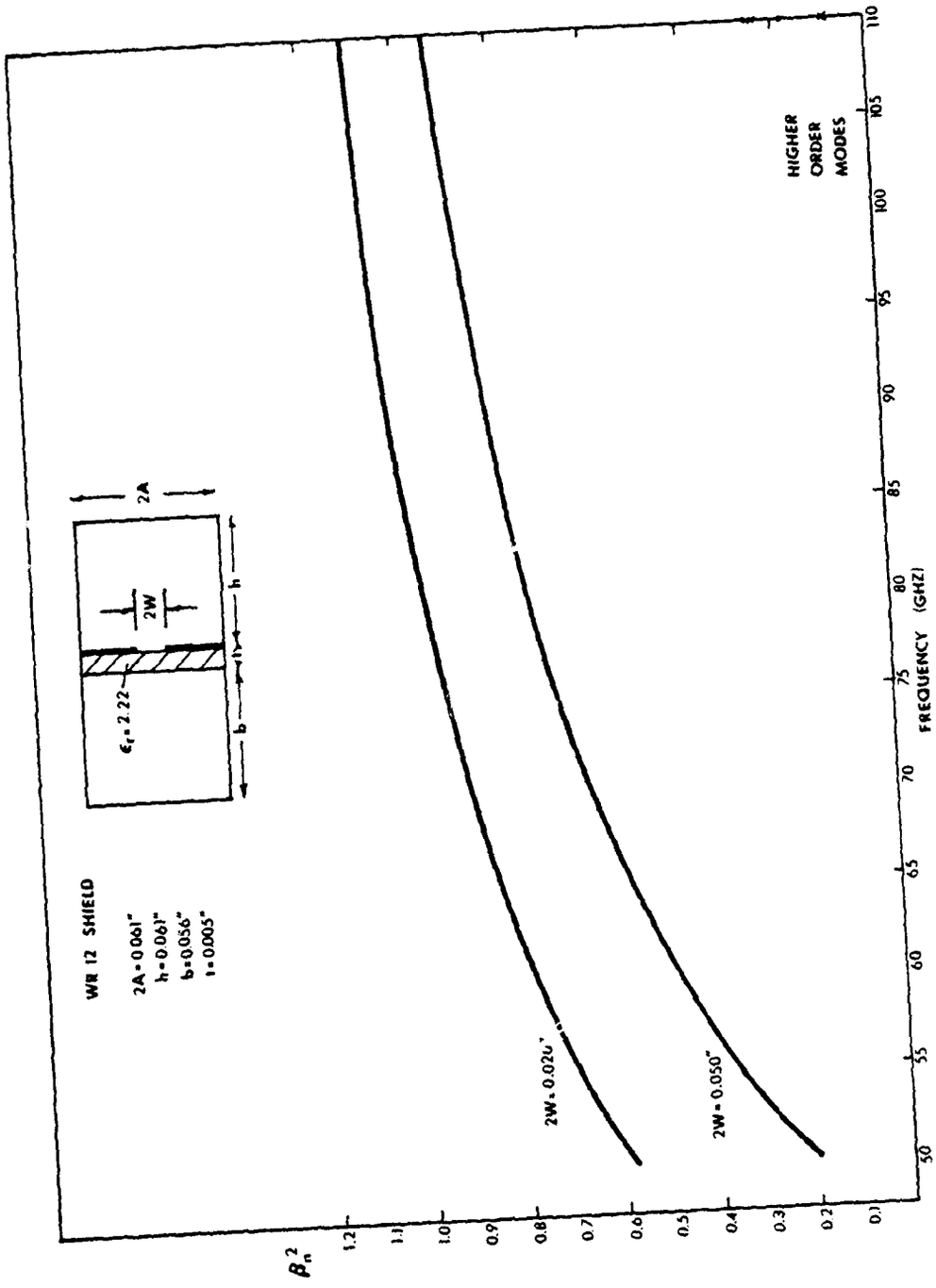

Figure 6. Dispersion Characteristics for Fin-line Shielded in WR12 Waveguide.

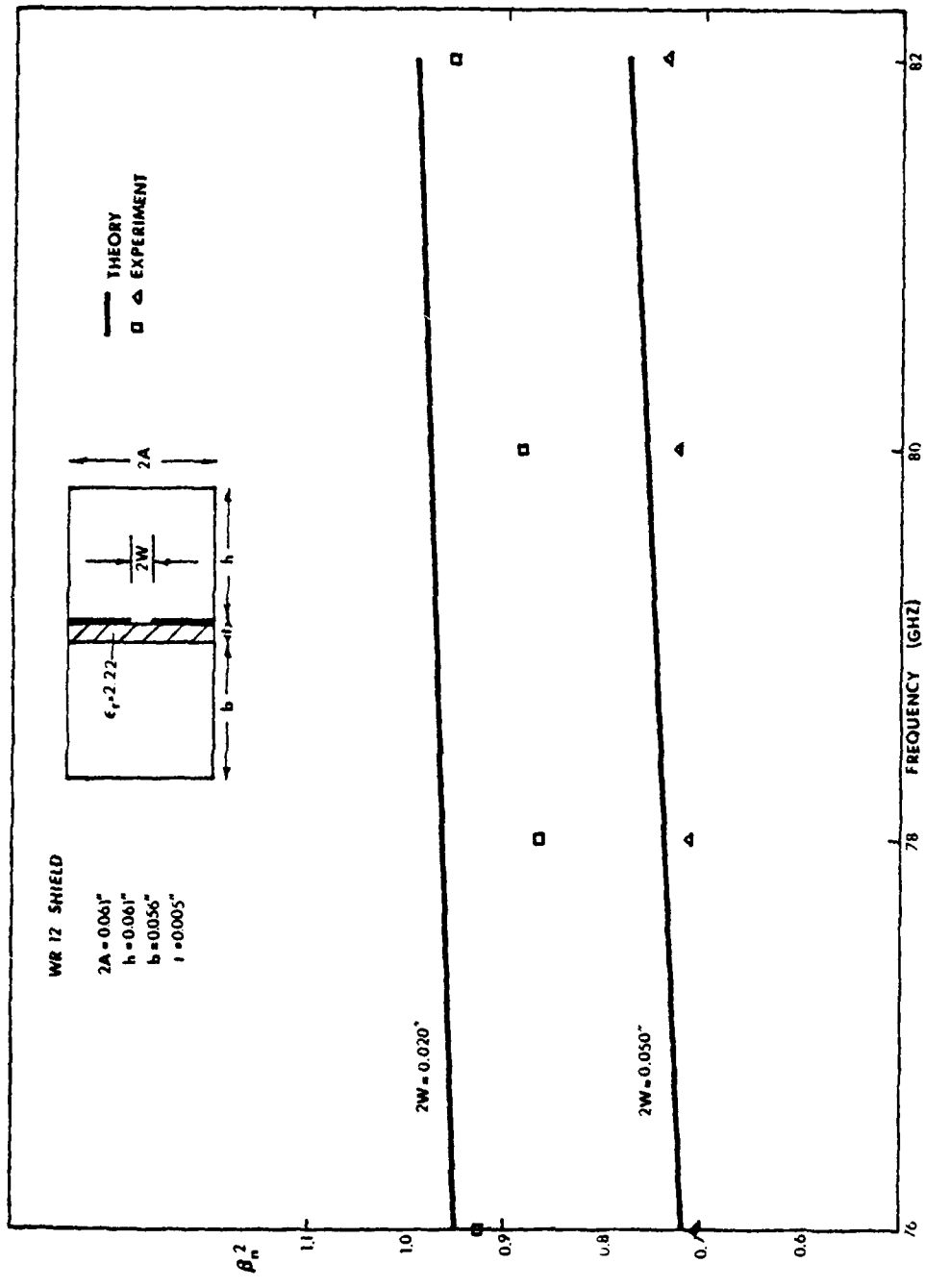

Figure 7. Comparison of Experimental and Theoretical Dispersion Characteristics.

A number of factors may have contributed to the discrepancy between measured and calculated values. Various experimental errors may have been present including the inability to machine the metal shield to exacting tolerances, and misalignment between the waveguide housing, the fin-line insert, and the sliding short. In addition, the theory assumes that the metal fins are infinitely thin and the metal fins and shield are perfect conductors.

Recently, Beyer and Wolff[14] have shown that the propagation constant is reduced when finite metallization of the fins is considered. Using a similar configuration, they show that the normalized propagation constant squared is reduced by approximately four percent for the case 2W = 0.020", but less than one percent for the case 2W = 0.050". The results shown in figure 7 are consistent with Beyer's and Wolff's results; however, it is impossible to conclude that the discrepancies are due entirely to finite metallization of the fins.

Figure 8 shows dispersion characteristics for two configurations of fin-line shielded in WR28 waveguide. An attempt was made to experimentally verify the curves shown, however, usable standing wave patterns were not obtained.

C. Experimental Data and Numerical Data, Multi-Mode Case

Propagation constants were measured for a number of multi-moded configurations in an effort to characterize the effects of

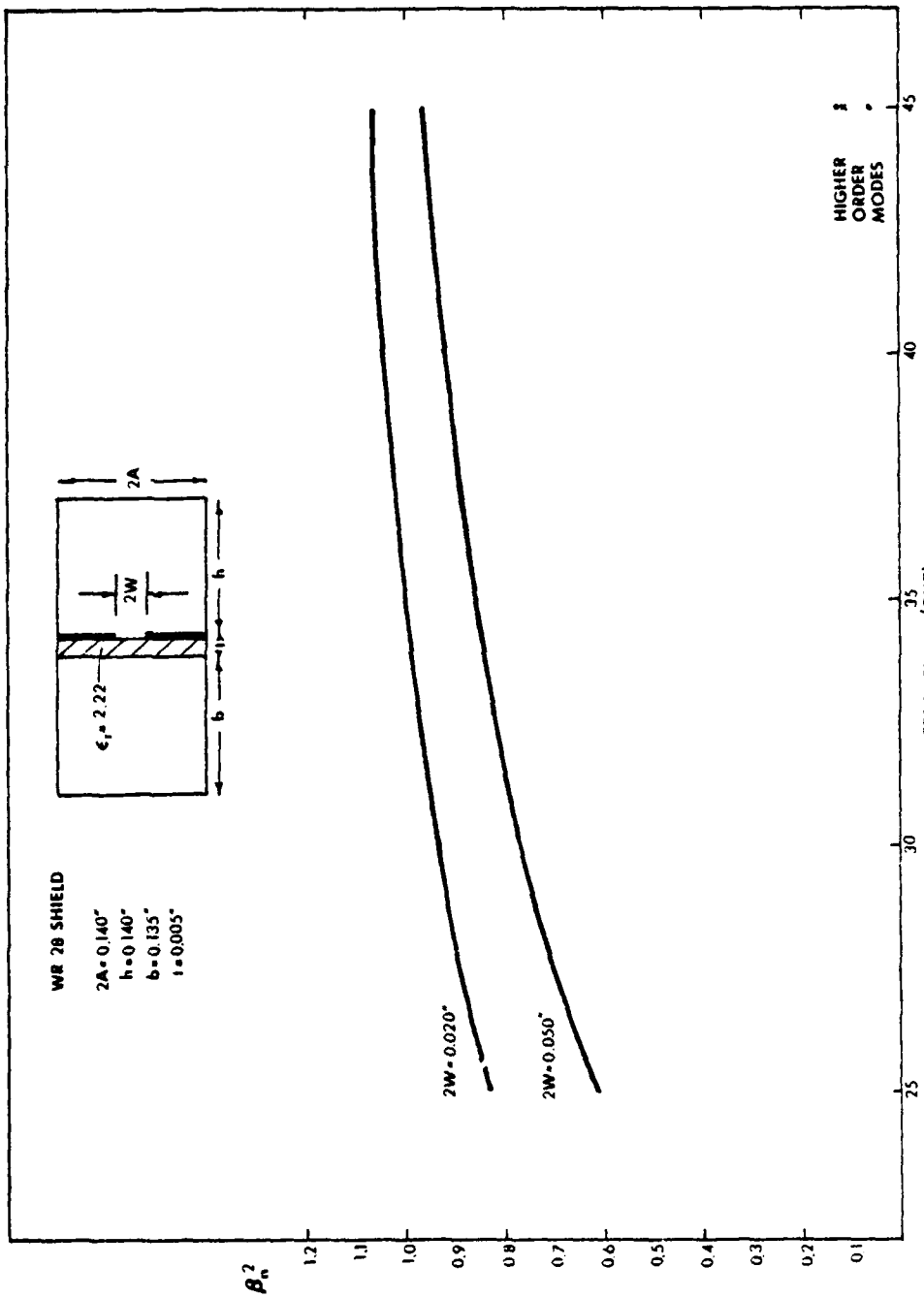

Figure 8. Dispersion Characteristics for Fin-line Shielded in WR28 Waveguide.

the higher order modes. The dispersion characteristics of the dominant and higher order modes are illustrated in figure 9 for WR28 shield and 2W = 0.020", in figure 11 for WR28 shield and 2W = 0.050", in figure 13 for WR90 shield and 2W = 0.020", and in figure 15 for WR90 shield and 2W = 0.050". For each case above experimental values along with theoretical curves are given in figures 10, 12, 14, and 16, respectively. In each case only the first few higher order modes are plotted; many other higher order modes occur below the first few but are not shown.

A smooth transition between the WR12 feed waveguide and the fin-line section was only available for the WR90 shield. The fin-line section using a WR28 shield was illuminated by an open ended section of WR12 waveguide.

As illustrated in figures 10 and 12, for WR28 shield the measured values fall within a few percent of the dominant mode. This is consistent with the standing wave patterns that showed no observable beat pattern that would occur if power were being coupled into the higher order modes. Whether or not higher order modes contribute to the standing wave pattern will depend on the way the fin-line is illuminated, the type of sliding short used, and any experimental errors that attenuate or amplify the higher order mode contributions. Assuming that the sliding short reflects any higher order modes, negligible power is coupled into the higher order modes for the two configurations shown in figures 9 through 12.

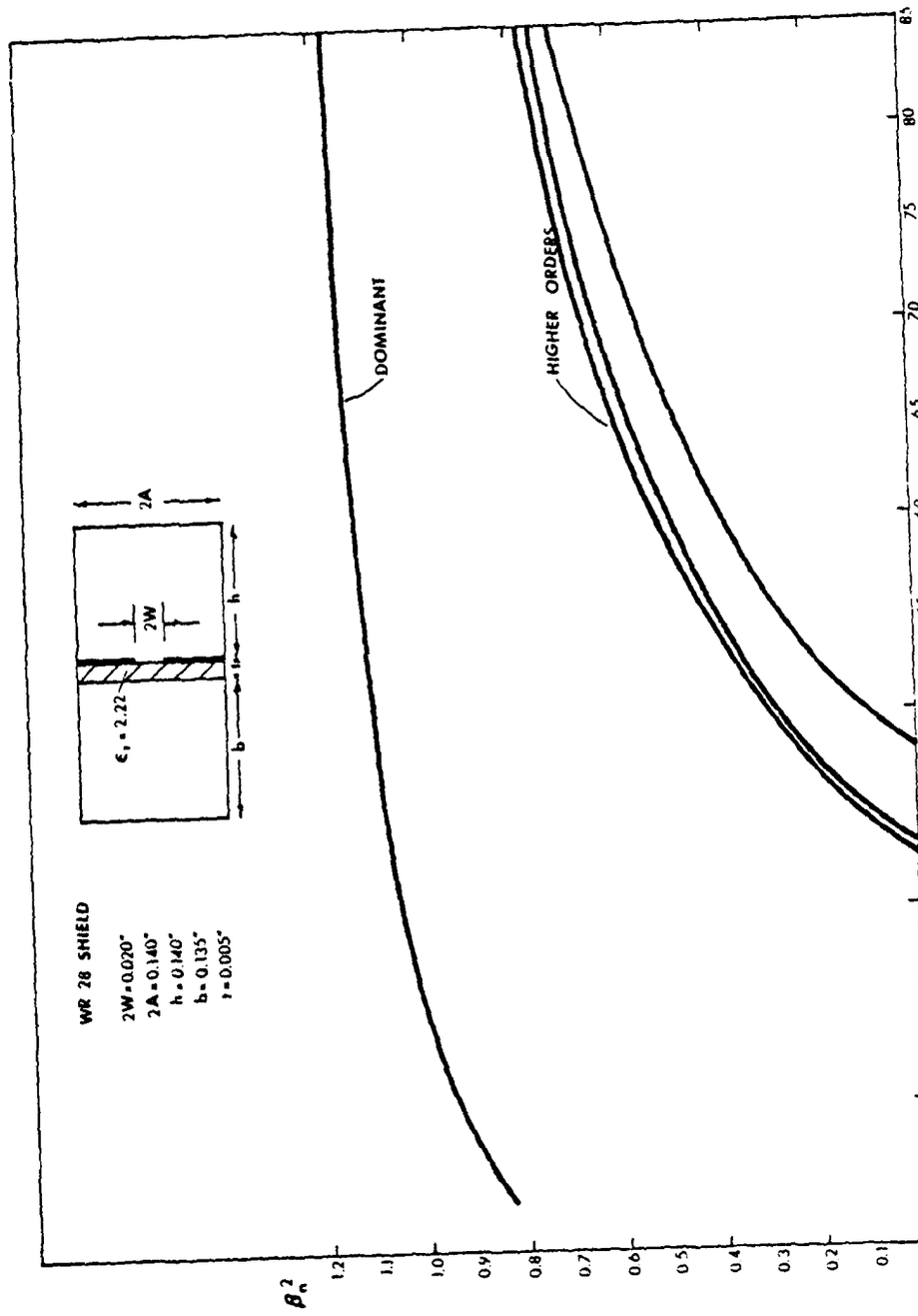

Figure 9. Dispersion Characteristics of Dominant and Higher Order Modes WR28 Shield 2W = 0.020".

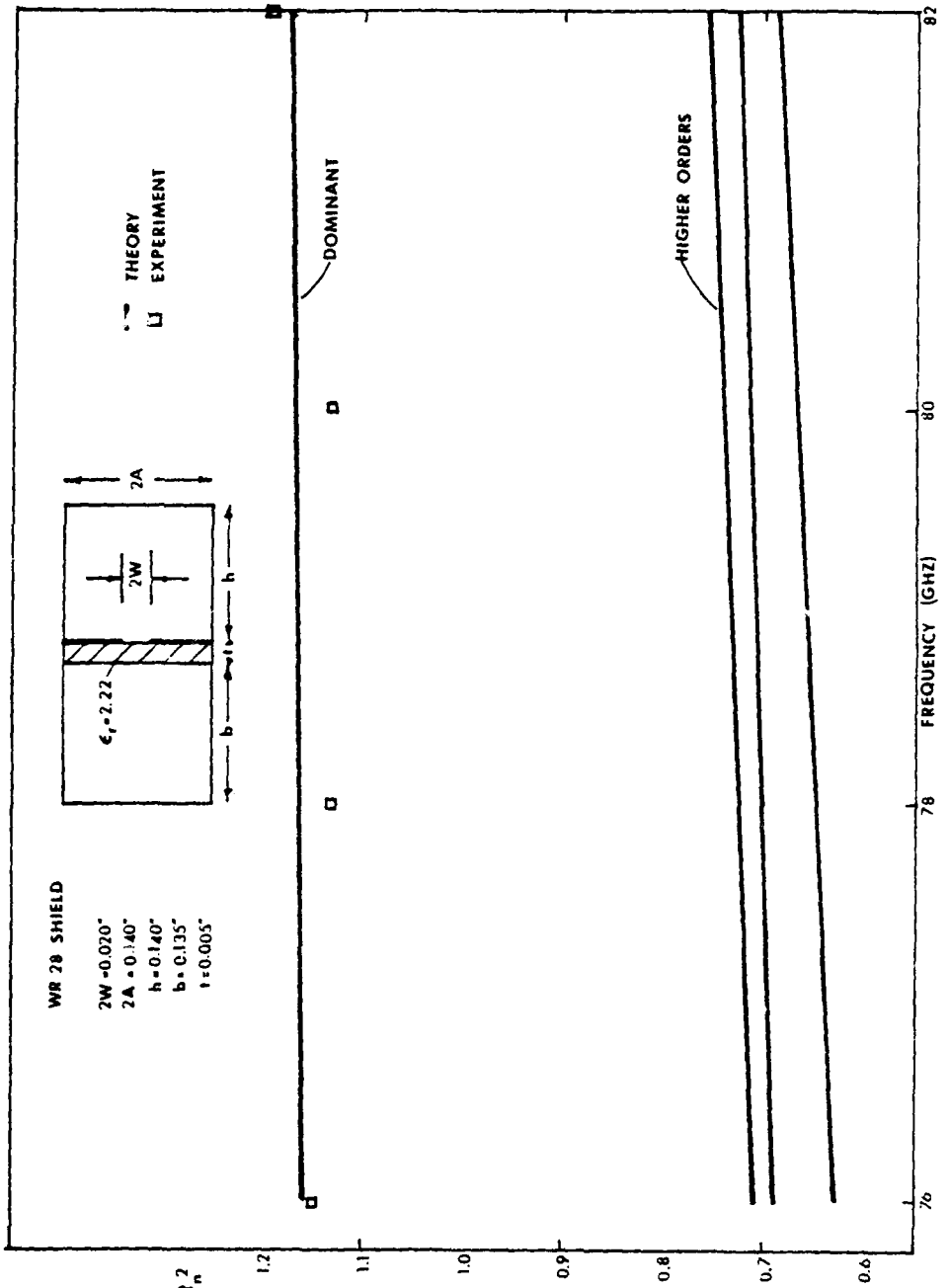

Figure 10. Experimental Values and Theoretical Curves WR28 Shield 2W = 0.020".

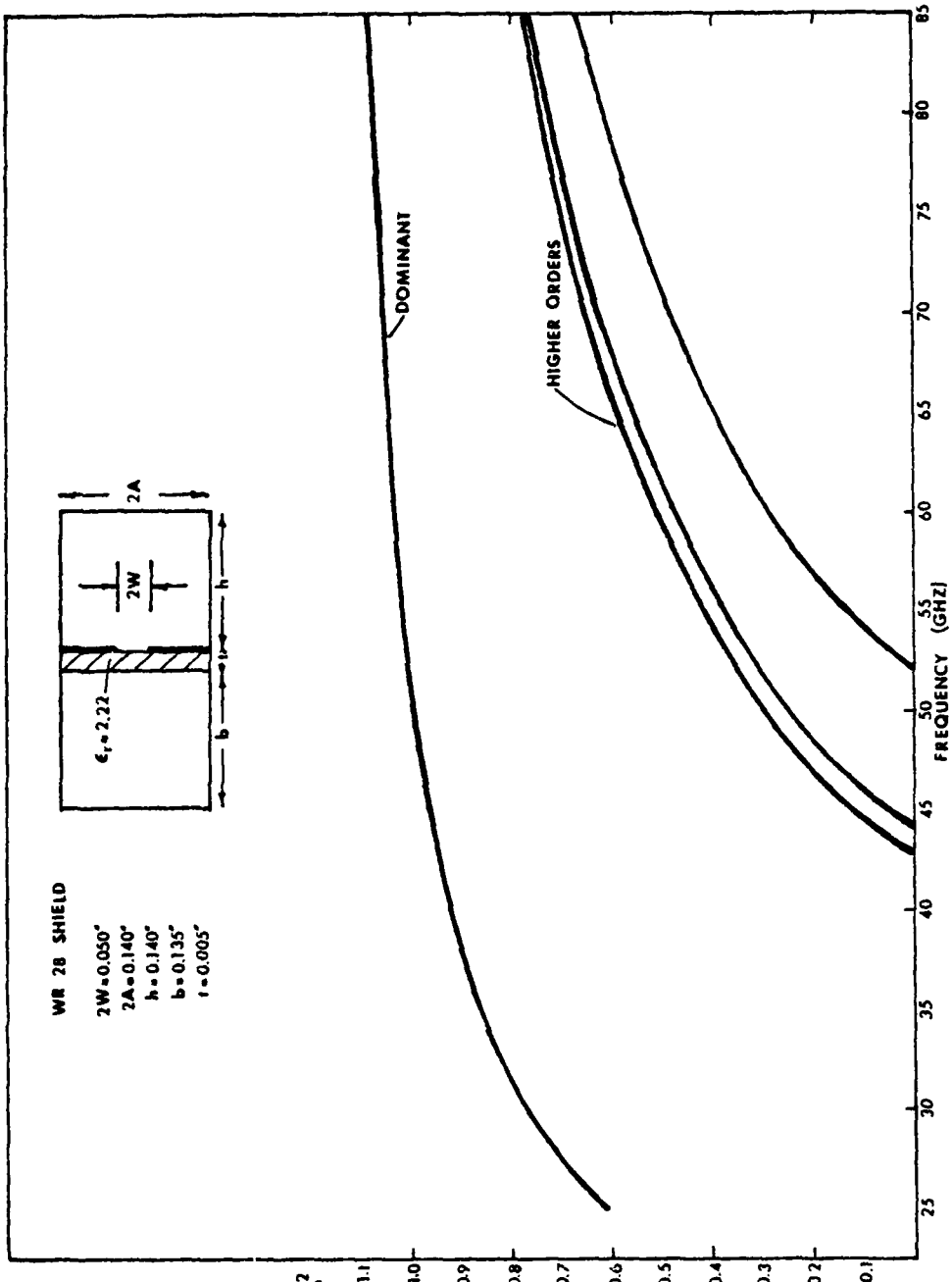

Figure 11. Dispersion Characteristics of Dominant and Higher Order Modes WR28 Shield 2W = 0.050".

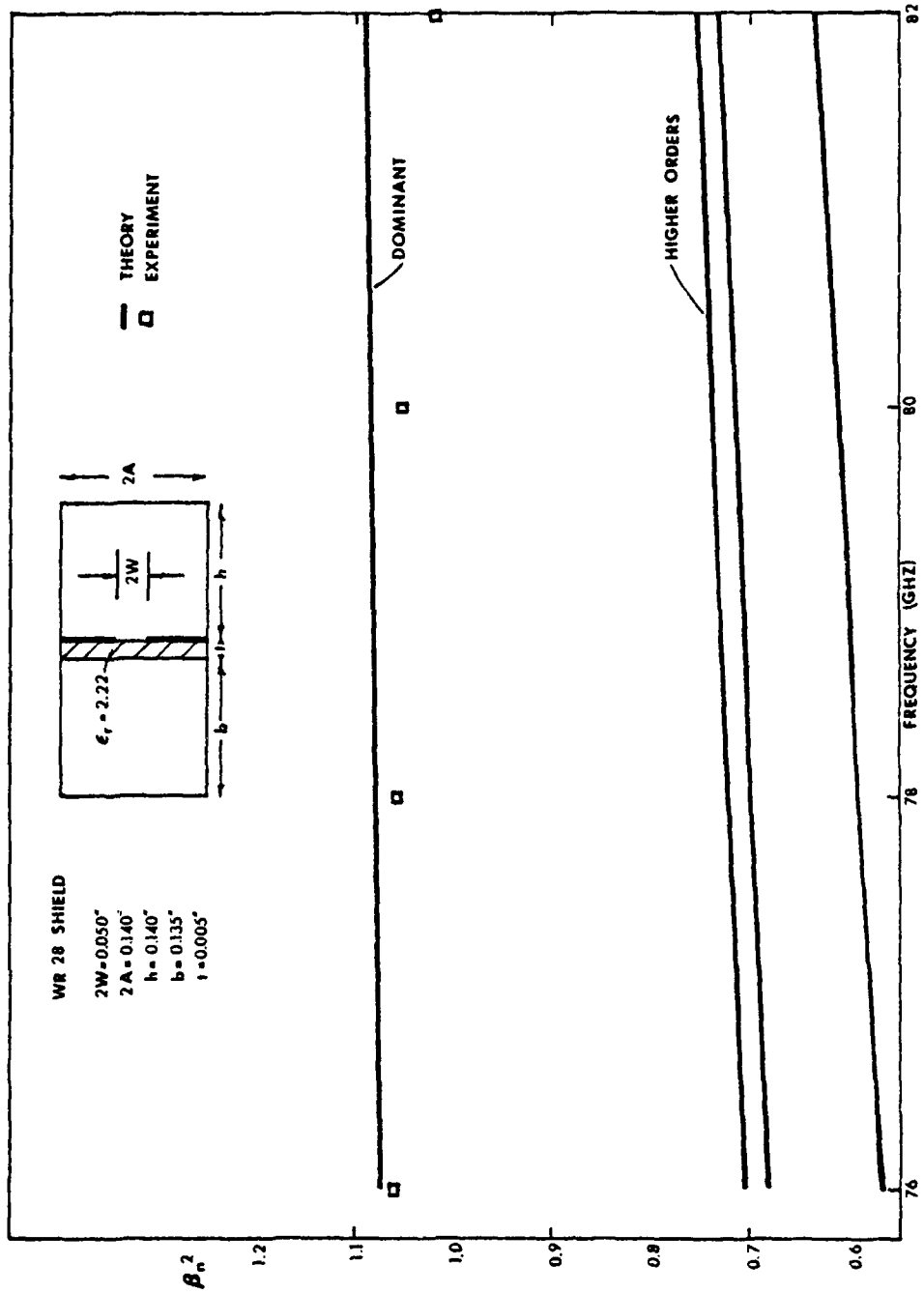

Figure 12. Experimental Values and Theoretical Curves WR28 Shield 2W = 0.050".

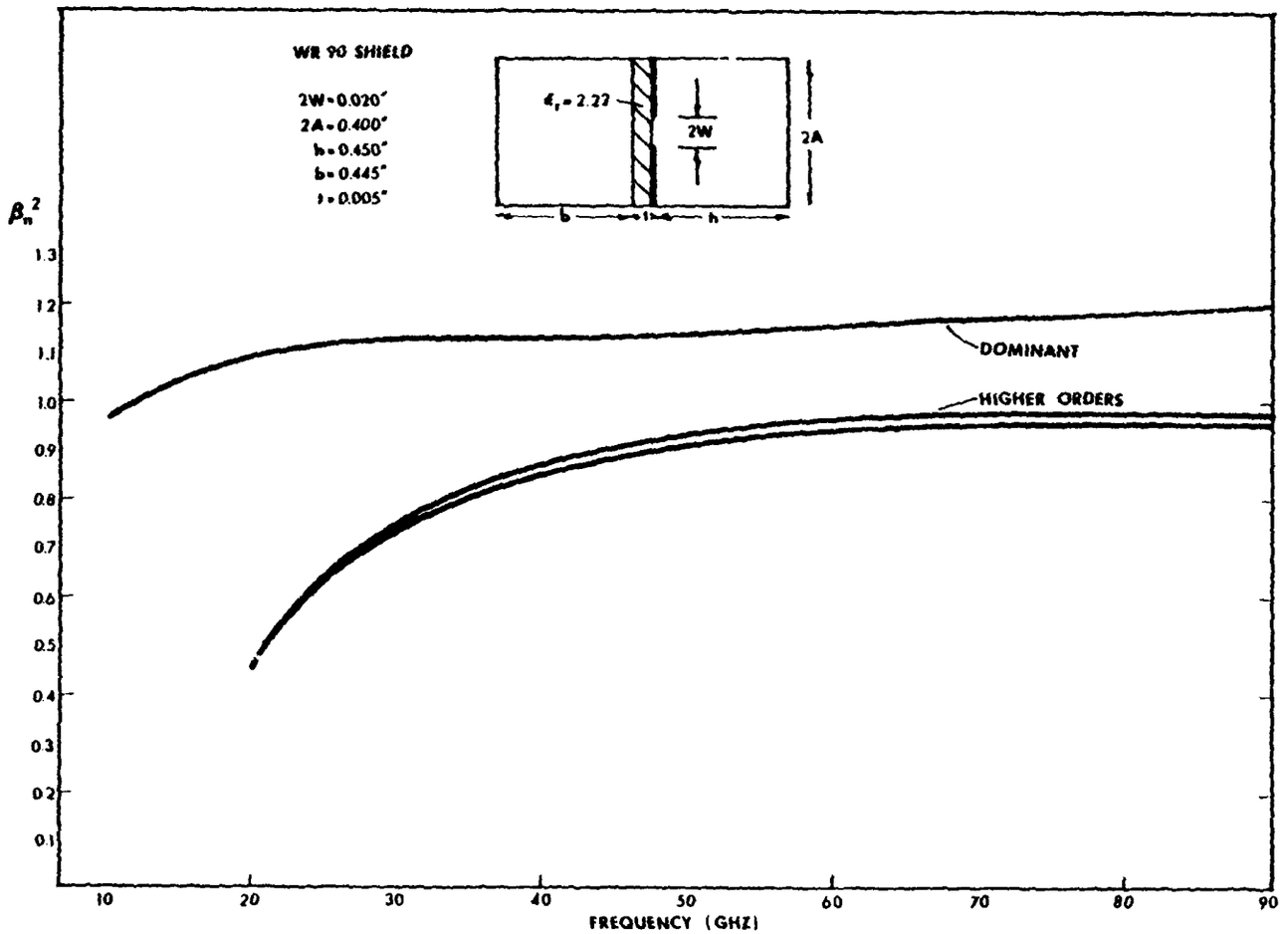

Figure 13. Dispersion Characteristics of Dominant and Higher Order Modes WR90 Shield 2W = 0.020".

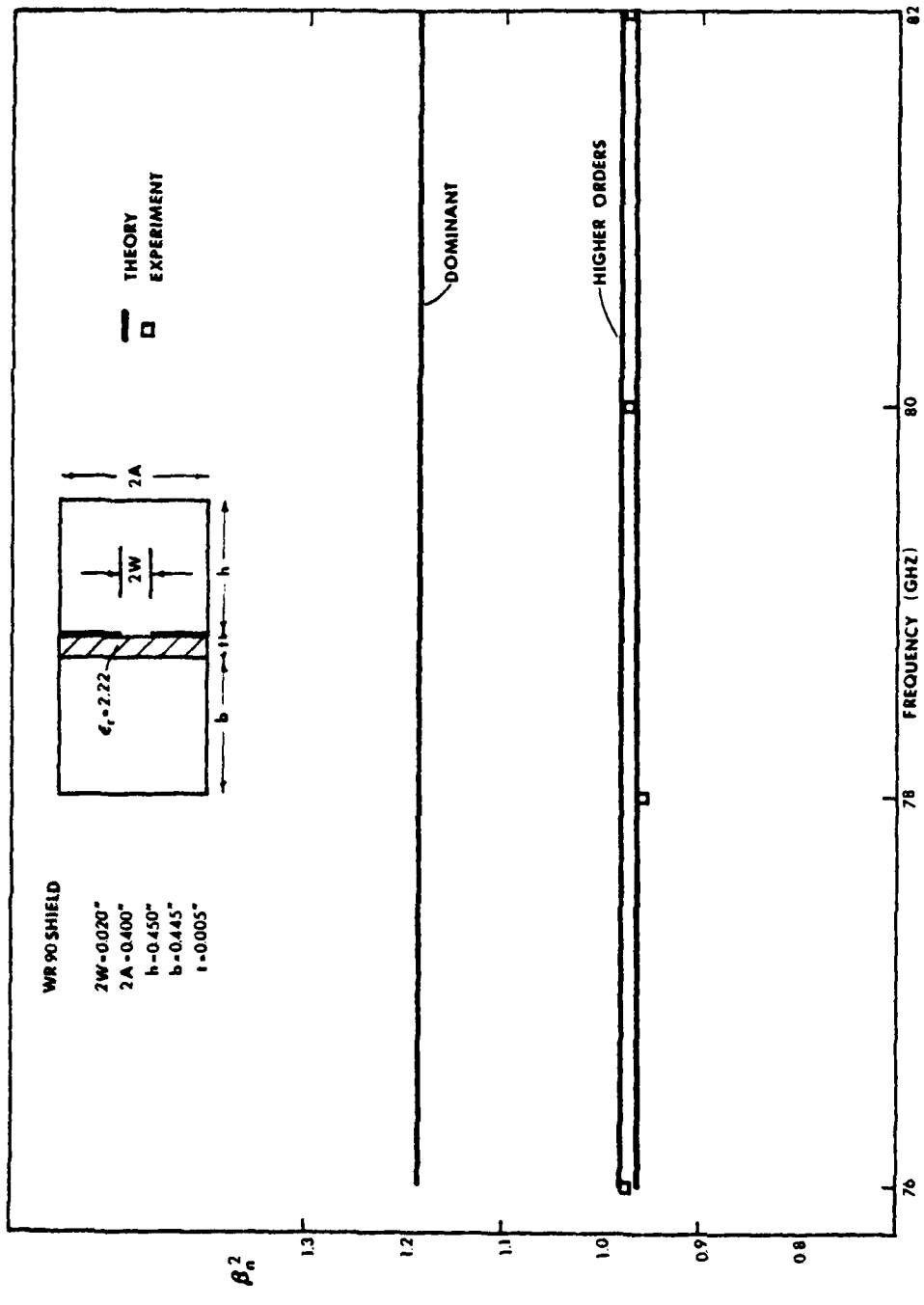

Figure 14. Experimental Values and Theoretical Curves WR90 Shield 2W = 0.020".

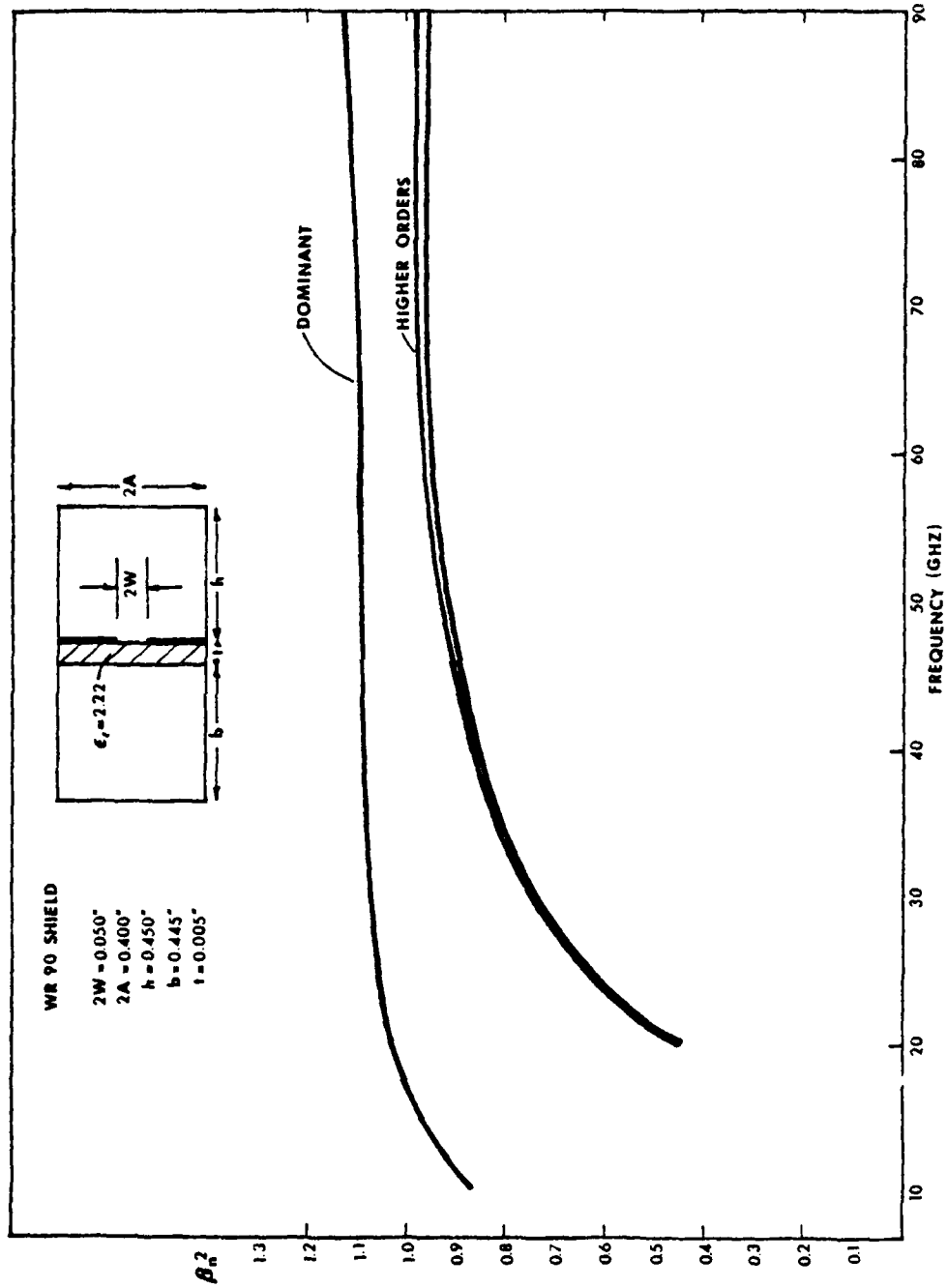

Figure 15. Dispersion Characteristics of Dominant and Higher Order Modes WR90 Shield 2W = 0.050".

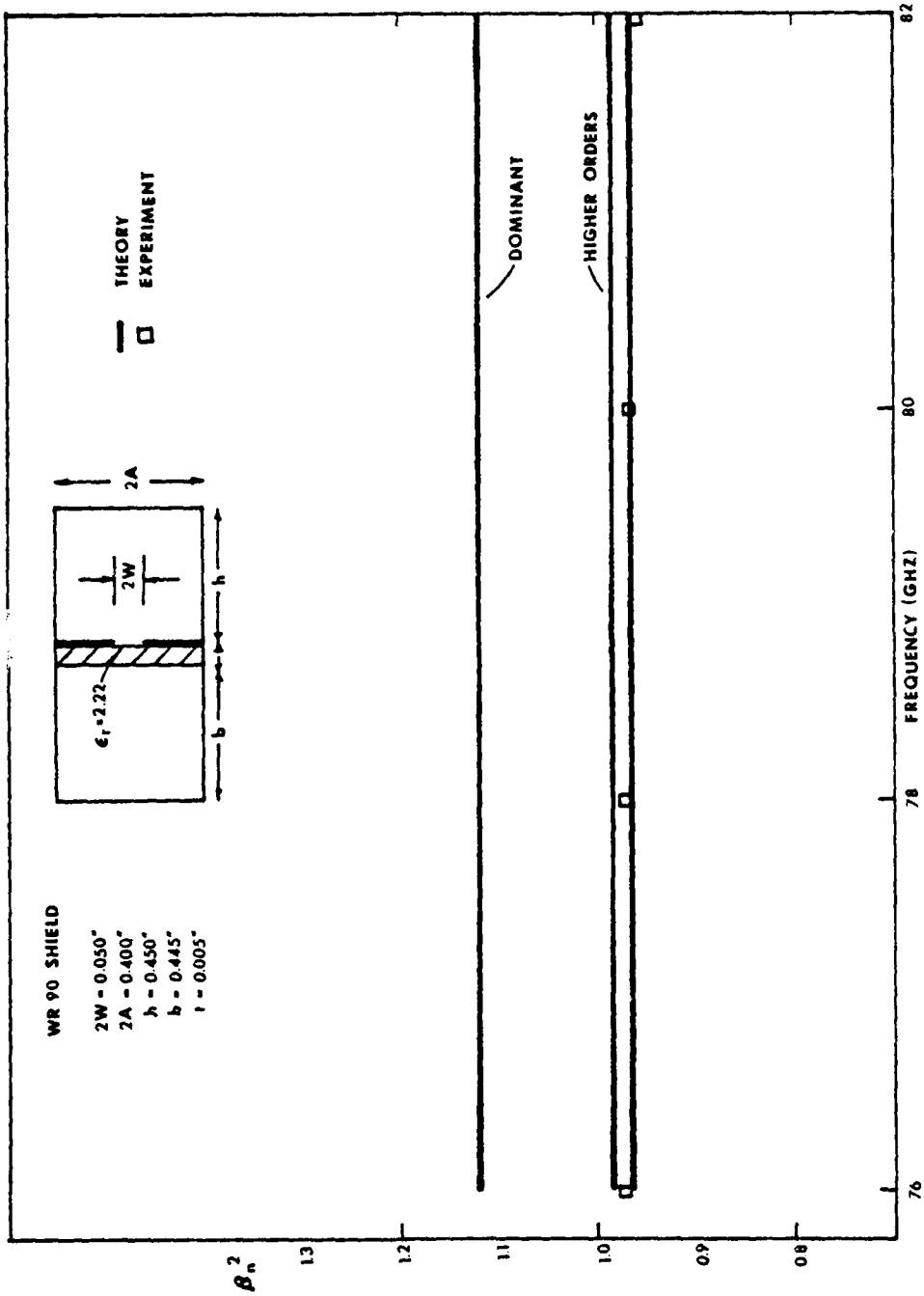

Figure 16. Experimental Values and Theoretical Curves WR90 Shield 2W = 0.050".

As illustrated in figures 14 and 16, for WR90 shield the measured values fall within a few percent of the first higher order mode. Because of random variations associated with the standing wave pattern, it was difficult to discern any beat pattern. The beat pattern is further complicated since a number of higher order modes are present. In most of the standing wave patterns for the WR90 shield configurations, a small amplitude beat pattern occurred.

The results suggest that single mode operation may be extended beyond the cutoff frequency of the first higher order mode. This behavior may depend on the method of excitation, and may not hold for fin-line excited by something other than the TE_{01} mode of metal waveguide.

D. Calculation of Field Distributions

A computer program was written that calculates the six field components in the x = 0 plane. As discussed in Chapter Two, the dispersion characteristics for a given fin-line configuration contain even and odd modes. For even modes, which include the dominant mode, E_x, H_y and H_z are even functions of x, and H_x, E_y, and E_z are odd functions of x. For odd modes H_x, E_y, and E_z are even functions of x, and E_x, H_y and H_z are odd functions of x. The expressions for the fields, equation (21) of Chapter 2, converge rapidly for all values of z except around z = 0. In this region the calculated field strengths oscillate either side of the actual value as the

number of terms is increased. The field strengths were estimated by extrapolating from the values outside this region; this is shown in the figures below by a dashed line. The field strength plots do not show absolute differences as a parameter is varied, rather they serve to illustrate the differences in the shape of the field profiles.

The effect of varying the dielectric constant of the substrate is illustrated in figure 17. As the dielectric constant increases the fields are concentrated more in the substrate. Since H_y and H_z are out of phase by one quarter of a cycle, a region of circular polarization exists where H_y and H_z are approximately equal. As illustrated in figure 17, as the dielectric constant of the substrate increases, this region of circular polarization becomes broader. This information is useful in the design of ferrite devices since a broad or a sharp region of circular polarization may be required.

The effect of decreasing the gap width is shown in figure 18. The fields are more concentrated in the substrate for smaller gap widths.

Figures 19 and 20 illustrate the effect of increasing frequency, and include the field distribution of the third higher order mode. The third higher order mode is the first even higher order mode, and therefore the first higher order mode with nonzero E_x, H_y, and H_z in the $x = 0$ plane.

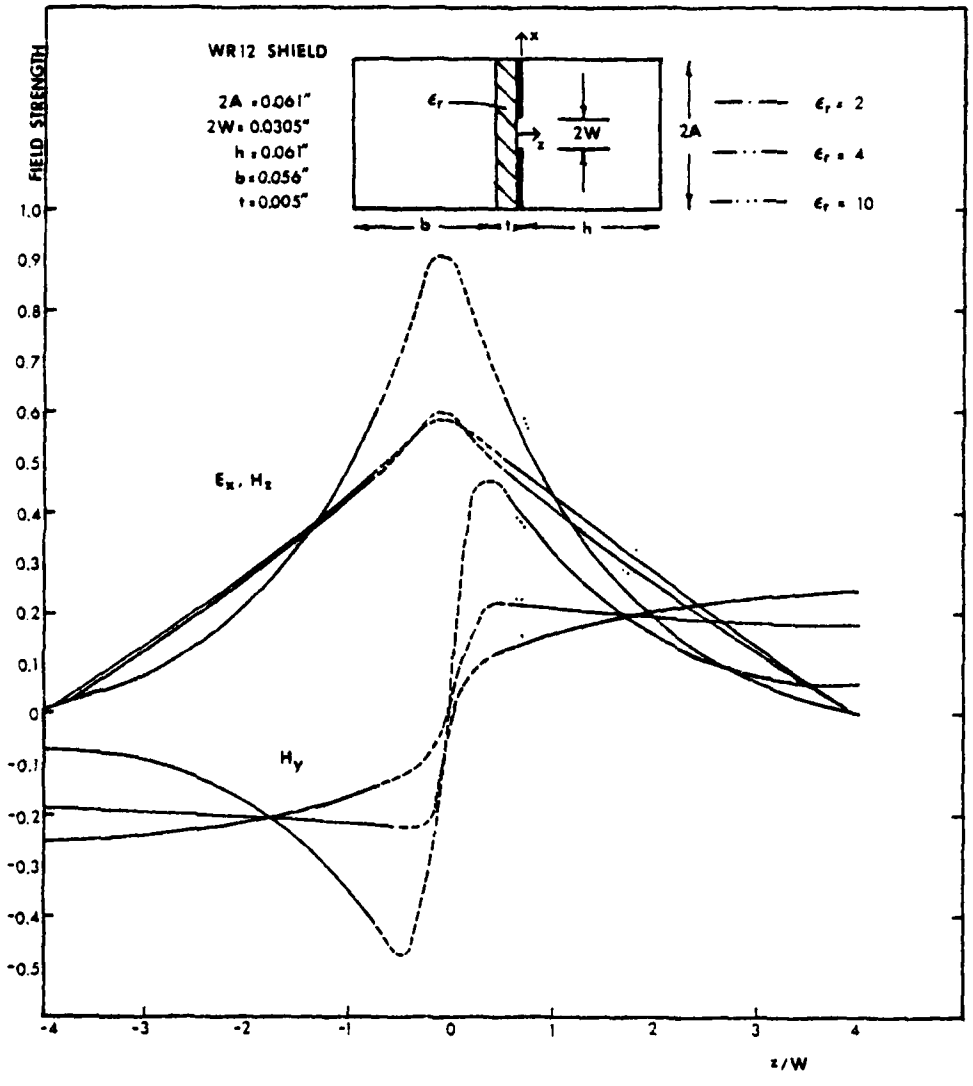

Figure 17. Field Distributions for Three Values of the Substrate Dielectric Constant.

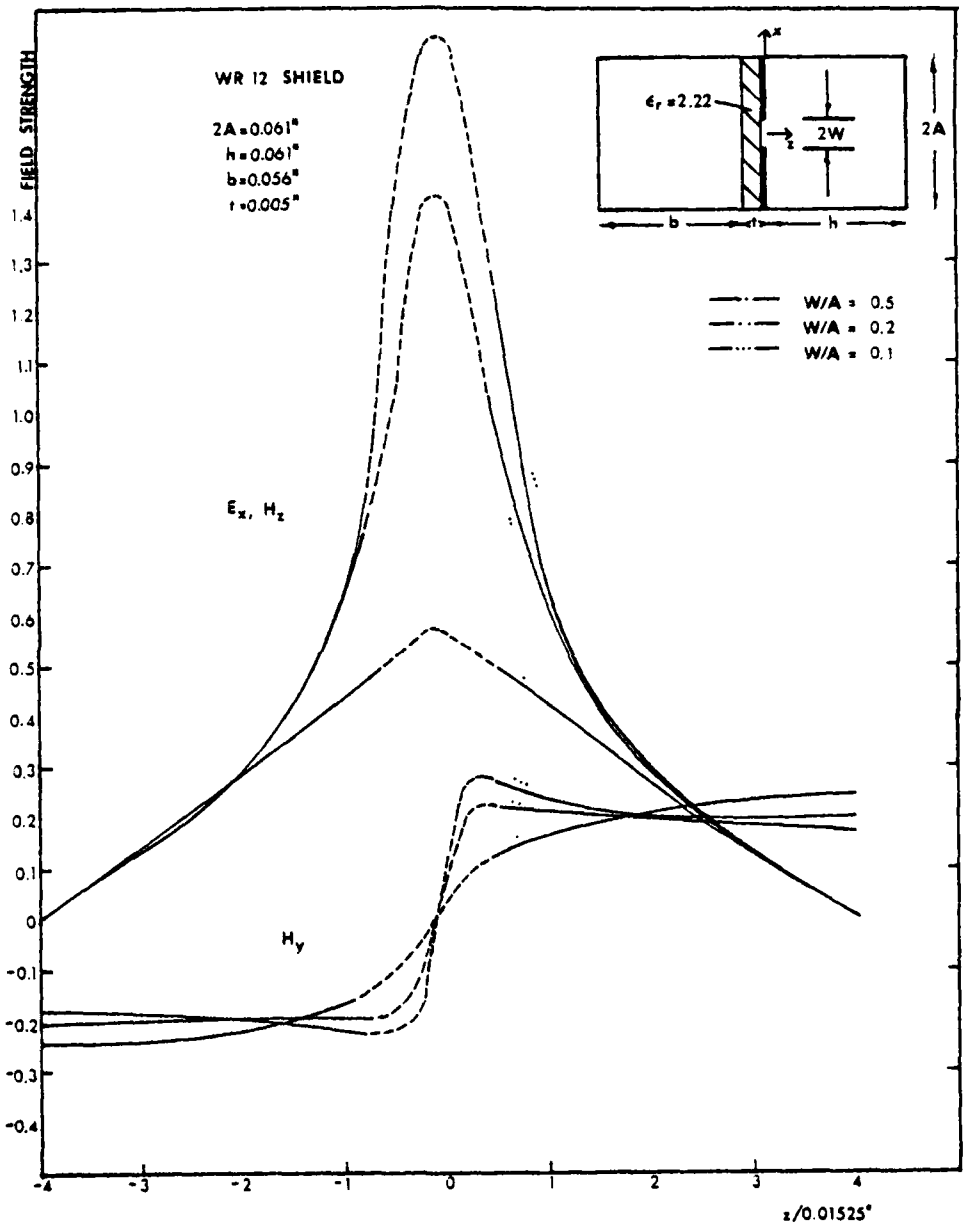

Figure 18. Field Distributions for Three Values of the Gap Width 2W.

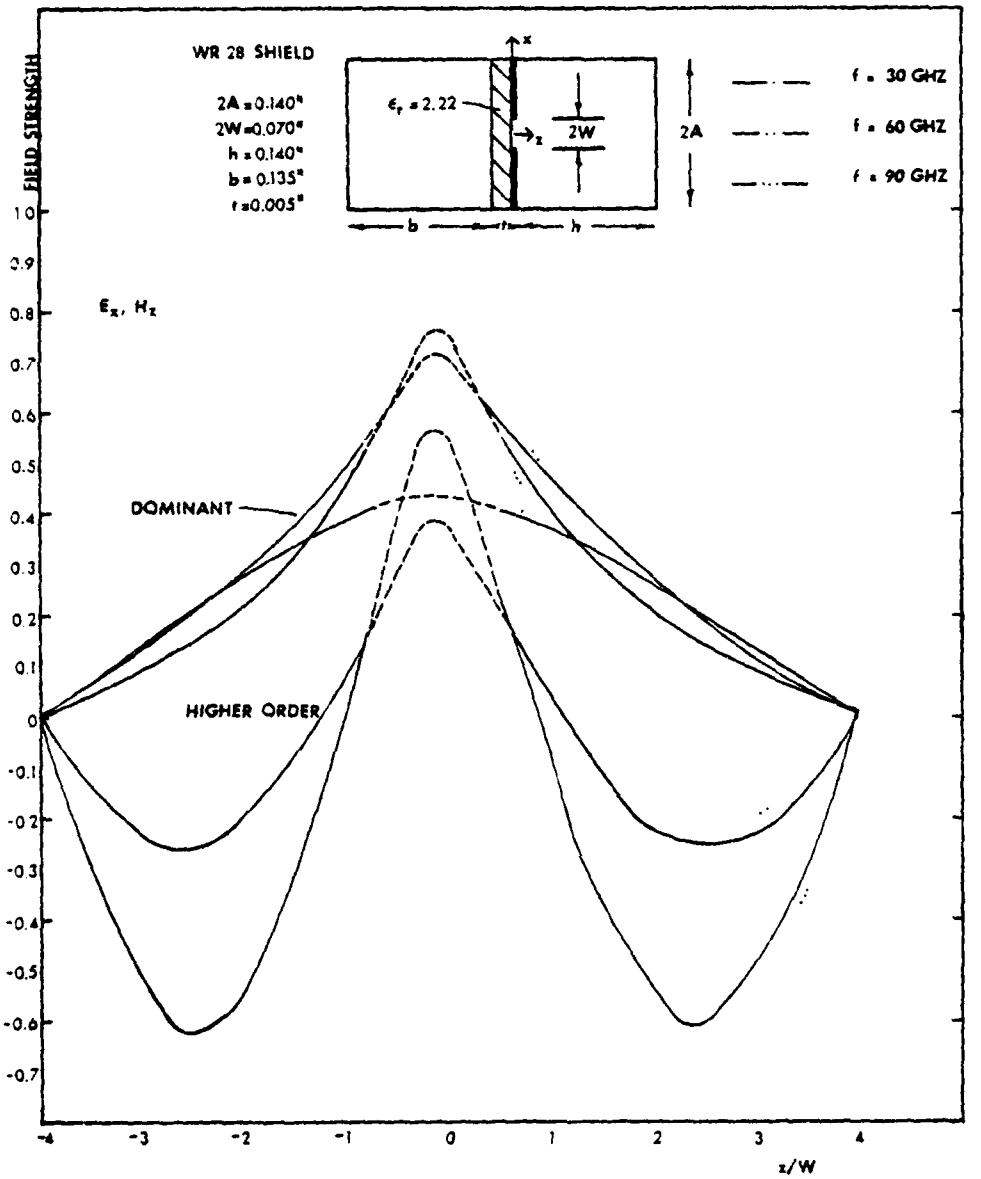

Figure 19. Dominant and Higher Order Mode Field Distributions at Three Frequencies E_x and H_z components.

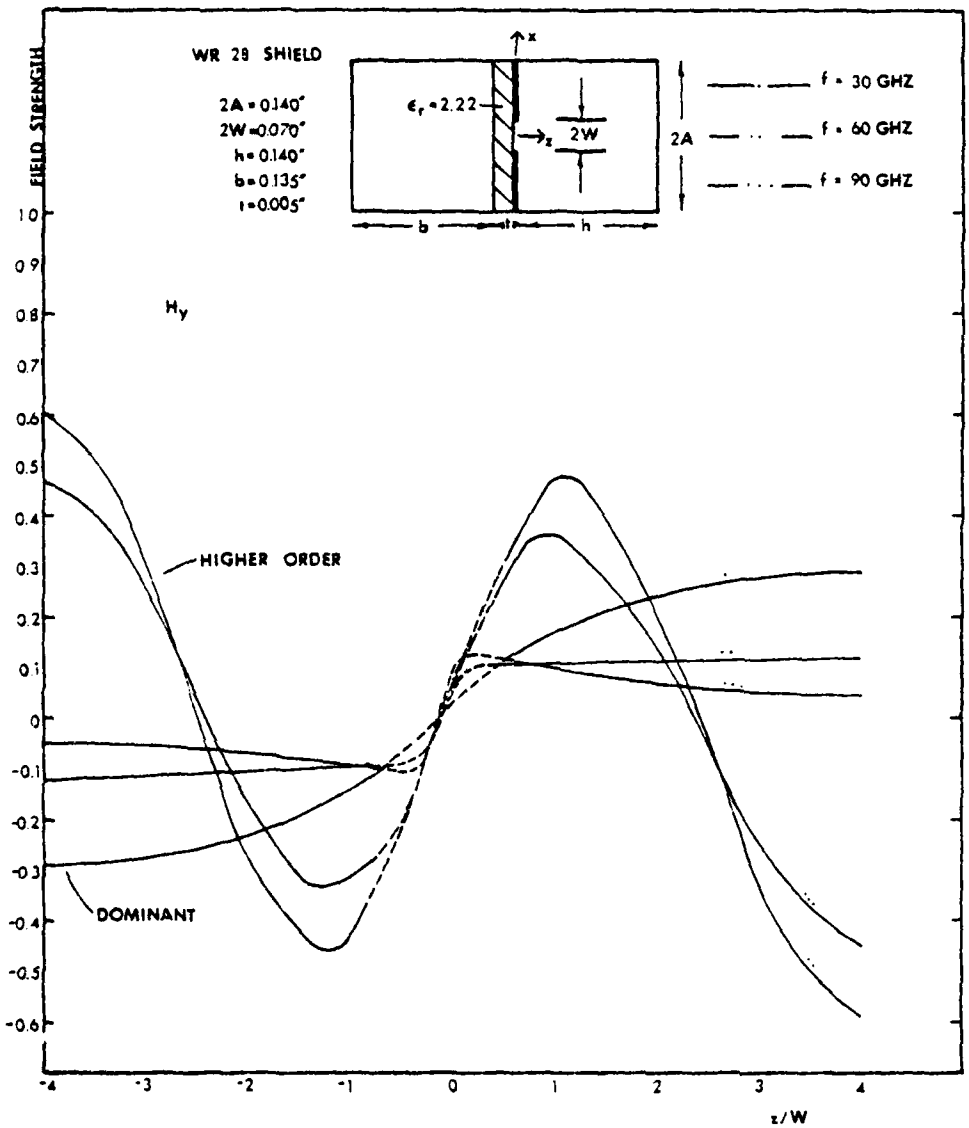

Figure 20. Dominant and Higher Order Mode Field Distributions at Three Frequencies H_y Component.

IV. CONCLUSIONS

The dispersion characteristics of a number of fin-line configurations have been given and an experiment was performed to experimentally verify the dispersion characteristics of these configurations. The results suggest that single-mode operation may extend beyond the cutoff frequency of the first higher order mode. If this is true, single-mode devices such as filters and couplers would be less restricted by small shield sizes at higher frequencies. Further experiments need to be performed before conclusions can be drawn since the results may be a function of the experiment itself.

Field distributions have been given for a number of fin-line configurations. These results may be used in the design of fin-line components such as couplers and ferrite devices.

V. LIST OF REFERENCES

1. P.J. Meier, "Two New Integrated-Circuit Media with Special Advantages at Millimeter Wavelengths," IEEE G-MTT Symposium Digest, 1972, pp. 221-223.
2. P.J. Meier, "Integrated Fin-Line Millimeter Components." IEEE Trans. Microwave Theory Tech., Vol. MTT-22, No. 12, December 1974.
3. H. Hofmann, "Dispersion of Planar Waveguides for Millimeter-Wave Application," Arch. Elek. Übertragung., Vol. 31, No. 1, January 1977.
4. A.M.K. Saad and K. Schunemann, "A Simple Method for Analyzing Fin-Line Structures." IEEE Trans. Microwave Theory Tech., Vol. MTT-26, No. 12, December 1978.
5. W. Hoefer, "Fin-Line Parameters Calculated with the TLM Method," IEEE MTT-S Symp. Dig., May 1979.
6. T. Itoh, "Spectral Domain Analysis of Dominant and Higher Order Modes in Fin-Lines," IEEE Symp. Dig., May 1979.
7. J.B. Knorr and P.M. Shayda, "Millimeter-Wave Fin-Line Characteristics." IEEE Trans. Microwave Theory Tech., Vol. MTT-28, No. 7, July 1980.
8. A.-M.A. El-Sherbiny, "Exact Analysis of Shielded Microstrip Lines and Bilateral Fin Lines," IEEE Trans. Microwave Theory Tech., Vol. MTT-29, No. 7, July 1981.
9. Y. Hayashi, Mittra and Farr, To Be Published.

10. P.J. Meier, "New Developments with Integrated Fin-Line and Related Printed Millimeter Circuits." IEEE MTT Symp. Dig., 1975.

11. H. Hofmann, H. Meinel, and B. Adelseck, "New Integrated Millimeter-Wave Components Using Fin-Lines." IEEE MTT Symp. Dig., 1978.

12. H.E. Hennaway and K. Schünemann, "Computer-Aided Design of Fin-Line Detectors, Modulators, and Switches," Arch. Elek. Übertragung., Vol. 36, No. 2, February 1982.

13. F. Arndt, J. Bornemann, D. Grauerholz, and R. Vahldieck. "Theory and Design of Low-Insertion Loss Fin-Line Filters," IEEE Trans. Microwave Theory Tech., Vol. MTT-30, No. 2, February 1982.

14. A. Beyer and I. Wolff, "A Solution of the Earthed Fin Line with Finite Metallization Thickness," IEEE MTT Symp. Dig., 1982.

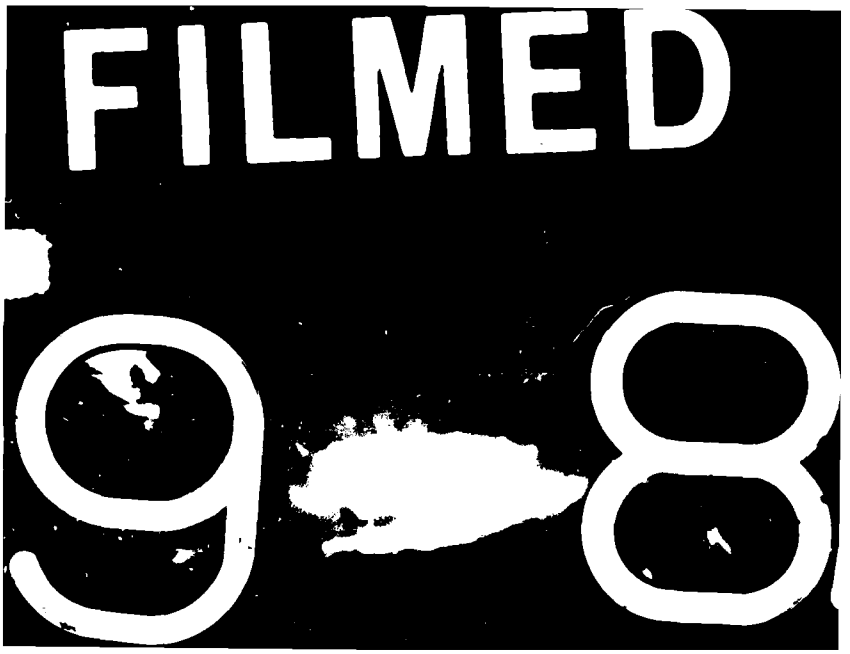
FILMED
9 8